applied sciences

MDPI

Article

Design Procedures for Sustainable Structural Concretes Using Wastes and Industrial By-Products

Ana Neves [1,*], João Almeida [1], Fábio Cruz [1], Tiago Miranda [1,*], Vítor M. C. F. Cunha [1], Mafalda Rodrigues [2], José Costa [2] and Eduardo B. Pereira [1,*]

[1] ISISE, Institute of Science and Innovation for Bio-Sustainability (IB-S), Department of Civil Engineering, University of Minho, 4800-058 Guimarães, Portugal
[2] DST Group, Rua de Pintancinhos—Palmeira, 4700-727 Braga, Portugal
* Correspondence: id6951@alunos.uminho.pt (A.N.); tmiranda@civil.uminho.pt (T.M.); eduardo.pereira@civil.uminho.pt (E.B.P.)

Abstract: The protection of the environment must be a priority in our society, and the construction sector can contribute significantly to this goal. Construction, being one of the industrial sectors that is more demanding in terms of raw materials, must reinforce its effort to implement, in a more profound and systematic way, the paradigm of the circular economy. In this sense, in recent years several studies have been trying to contribute solutions aimed at reintroducing industrial by-products or residues in new products for the construction industry. It should be noted that nowadays it is increasingly important to introduce a higher percentage of recycled materials in concrete. In this context, the present work addresses the appropriateness of a design procedure proposed to maximize the content of electric arc furnace slag (EAFS) and include recycled tire steel fibers (RTSF) in the production of more sustainable structural concretes. For this, the properties of various concrete mixtures at the fresh and hardened state, obtained by the substantial substitution of coarse and fine natural aggregates by EAFS and fly ash (FA), were investigated. The design of EAFS mixtures was based on two conventional reference mixtures (REF1 and REF2), and by using the modified Andreasen and Andersen particle packing model, these were optimized to achieve maximum packing density. Compressive strength, modulus of elasticity behavior, and fresh and physical properties were assessed in order to define the best mix proportions with respect to the predefined requirements of ordinary mixtures. Untreated recycled tire steel fibers (RTSF) were included in the developed sustainable concrete to perform a comparison of the physical properties with unreinforced concretes developed with natural aggregates (REF2) and with EAFS aggregates (EAFS8D1). This incorporation was intended to improve the physical behavior of unreinforced concretes with EAFS aggregates. Mixtures with high percentages of waste aggregates up to 70% (in weight), and 10% (in weight) of FA were obtained, showing competitive mechanical behavior compared to REF1 and REF2. These concrete compositions showed minimum and maximum compressive strengths between 9 MPa and 37 MPa, respectively. This study coverd the two major classes of concrete used as structural material, namely structural concrete and fiber reinforced concrete.

Keywords: recycled materials; industrial by-products; electric arc furnace slag; fly ash; recycled tire steel fibers; particle packing model; mechanical properties; durability; technological properties

check for updates

Citation: Neves, A.; Almeida, J.; Cruz, F.; Miranda, T.; Cunha, V.M.C.F.; Rodrigues, M.; Costa, J.; Pereira, E.B. Design Procedures for Sustainable Structural Concretes Using Wastes and Industrial By-Products. *Appl. Sci.* **2023**, *13*, 2087. https://doi.org/10.3390/app13042087

Academic Editors: Sara Cattaneo and Manuela Alessandra Scamardo

Received: 10 January 2023
Revised: 30 January 2023
Accepted: 4 February 2023
Published: 6 February 2023

Copyright: © 2023 by the authors. Licensee MDPI, Basel, Switzerland. This article is an open access article distributed under the terms and conditions of the Creative Commons Attribution (CC BY) license (https://creativecommons.org/licenses/by/4.0/).

1. Introduction

The construction sector is a large contributor to the problems of global warming, responsible for about 30% of the total greenhouse gas emissions that are released into the atmosphere annually. The construction process and the extraction of raw materials (including transportation) also consumes 25–45% of the total energy in OECD countries. Therefore, more sustainable solutions are increasingly important and desired by the construction industry to reduce its ecological footprint, and increase the application of the

paradigm of the circular economy in their activities [1–3]. A significant part of the current effort to pursue these more sustainable solutions involves research and innovation in the area of structural concrete. In fact, in recent years several studies have been carried out aiming at partially or totally replacing cement, natural aggregates, and fibers, or to replace natural supplementary cementitious materials (SCMs), by wastes, industrial by-products or recycled materials. Examples of wastes or recycled materials that were recently studied for incorporation into alternative structural concrete compositions as binders are fly ash, glycerol, cooking oil, ground granulated blast furnace slag (GGBS) and limestone powder, among others [4–6]. Additionally, there are other studies where recycled materials were introduced into concrete compositions as coarse and fine aggregates. Examples of these are electric arc furnace or blast furnace slag, plastics, quarrying, construction and demolition residues, textiles, ceramics, vegetable ash, pulverized fuel ash, municipal solid waste ash, silica fume and glass [7–10]. Recent studies also show the reuse of tire rubber and recycled tire fibers, respectively, as aggregate or fibers in concrete [11–16].

Fly ash (FA) is a fine mineral powder and is generated from the coal used in thermoelectric power plants, and therefore characterized as an industrial by-product. Its incorporation adds several advantages to concrete compositions such as: increased resistance to chemical attack and to the aggressiveness of different environments; increased long-term mechanical strength; reduction in shrinkage cracking and increased physical-mechanical concrete resistance [17–19]. However, fly ash is becoming a scarce product, as coal-based thermoelectric power plants are being discontinued.

Electric arc furnace slag (EAFS) is a waste product resulting from the steelmaking process in an electric arc furnace, where recycled steel scrap is melted. This material is characterized as a dense by-product [7,8,20]. Many of the studies conducted incorporating EAFS have found quite satisfactory results, and although some research may be found in this study area [21–26], it is still important to deepen this knowledge regarding the mechanical and durability properties, as well as on the design methodology. García-Cortés et al. [27] focused their research on the design of structural concrete compositions based on two discrete particle packing models, namely the compressible packing model and the 3-parameter particle packing model. Concrete compositions were designed to obtain the most compact structure of commercial natural limestone (NL) and EAFS aggregate. The water/cement (w/c) ratio was fixed equal to 0.55 to reach a concrete composition with a strength class above 30 MPa. The maximum content in solid weight of EAFS aggregates used were between 49.4% and 70.5%. It was concluded that the slump of all concrete mixtures designed with a cement amount of 260 kg/m^3 of concrete corresponded to a dry consistency. On the other hand, when a higher amount of cement was added to the concrete (i.e., 320 kg/m^3), the workability improved. They also confirmed the validity of using the particle packing models for the mixtures studied. Chatzopoulos et al. [28] showed that the replacement of conventional limestone aggregates in reference concrete mixtures, to produce concrete mixtures of C25/30 and C30/37 strength classes, by EAFS and ladle furnace slag (LFS) led to an improvement of their mechanical and physical properties, as well to their service life extension. In their study, they used a cement amount of 350 kg/m^3, w/c ratio of 0.51, and 30% and 50% of slag aggregates (EAFs and LFS) by volume. The increase in compressive strength at 7 days was 50% and in the case of frost resistance, after exposure, the scaling leads to a weight reduction 3.5 times lower than that of the reference concretes. These alternative concrete mixtures also showed reductions of CO_2 of 55% in natural carbonation and 40% in accelerated carbonation. The reduction of chloride penetration was of 57%. Additionally, they verified that the structures constructed with these alternative concrete mixtures resulted in a cost reduction per cubic meter of concrete of 35% per year of life, and a service life increase by up to 130%, considering the mechanism of deterioration due to chloride penetration. Other researchers did not find such favorable results in terms of physical properties compared to typical concretes, with a cement amount of 275 kg/m^3, as in the case of the previous study [29]. In fact, they verified that concrete mixtures with approximately 79% (in solid weight) of EAFS presented higher depth of water penetration

under pressure, due to the high porosity of EAFS aggregates, a slightly higher expansion, higher carbonation depth and similar resistance against freeze-thaw cycles in relation to reference mixtures. Furthermore, they recommend that attention must be paid to the case of components with high aesthetic demands, since these alternative concretes, when subjected to significant variations of humidity, showed stain points on the concrete surface due to the corroded iron nodules present in the EAFS particles. On the other hand, they concluded that concrete mixtures with EAFS aggregates presented similar and even higher compressive strength than reference concrete mixtures with limestone and with barite aggregates, respectively. Additionally, the fresh behavior was in accordance with the previous studies. Concrete mixtures with EAFS aggregates showed a lower slump value than the reference concrete mixtures, due to the increase in water absorption and the lack of fines in the EAFS aggregates.

In 2005 around 270,000 tons of EAFS were produced in Portugal, with an average of 110–150 kg of EAFS generated annually for each ton of liquid steel produced [30]. Moreover, it was estimated that about one billion end-of-life tires were discarded every year worldwide [31]. Hence, it is necessary to find a second use for these materials, which not only impact negatively on the environment but also on health in general. Therefore, and based on previous research available in the literature, this research was aimed at exploring the opportunity to assess the performance of the design approach proposed for designing concrete mixtures that will primarily be resourcing EAFS, as well as RTSF. The EAFS concrete compositions were defined using the modified Andreasen and Andersen particle packing model, envisaging the flexible adaptation of the design procedure to other types of waste materials or industrial by-products. After selecting the most satisfactory concrete compositions, i.e., the ones showing a lower residual sum of squares (*RSS*) and the best fit with the target or reference curve, the concrete properties were analyzed in the fresh and hardened state. Subsequently, recycled tire steel fibers (RTSF) were incorporated in the EAFS concrete selected with regard to the predefined requirements of ordinary mixtures, to maximize the incorporation and reuse of wastes that were not biodegradable, and to improve its mechanical and physical properties such as toughness, porosity at atmospheric pressure and under vacuum, sorptivity, permeability to air and water and carbonation resistance. A maximum content of 10% (in weight) of Fly Ash (FA) and 70% (in weight) of EAFS aggregates was used in concrete compositions whose minimum and maximum compressive strengths were between 9 MPa and 37 MPa, respectively. This research covered the two main types of concrete used in structural applications, namely structural concrete and fiber reinforced concrete.

2. Experimental Program

2.1. Materials

In this research two reference structural concretes (REF1 and REF2) were selected as the conventional mixtures. These two mixtures have distinct formulations, since the REF2 mixture has a lower cement amount relative to the REF1 mixture. Additionally, REF1 has no FA powder. The reference structural concrete REF1 showed a slump class S3 and was classified as of strength class C30/C37. The solid skeleton of REF1 was composed of natural aggregates with grain size fractions of 6–14 mm and 14–20 mm medium sand (0–4 mm) and fine sand (0–2 mm). Portland cement CEM II/A-L 42.5 R (CEM) was used as binder, and a plasticizer (PL) based on modified lignosulphonates and a last generation superplasticizer (SP) based on poly aryl ether (PAE) polymers (Master Builders) were used. The water/powder (w/p) and water/cement (w/c) ratios were equal to 0.54 and 0.59 (in weight), respectively. REF 2 was composed of the same ingredients mentioned above for the REF1 mixture although fly ash (FA_2) was also included, obtained from Pego Thermoelectric Power Plant. It was also designed to achieve a slump class of S4 (≈200 mm) and a strength class of C25/C30. The water/powder (w/p) and the water/cement (w/c) ratios were equal to 0.35 and 0.75 (in weight), respectively. During the project the FA was modified due to a supplier change, resulting in types of FA with two different densities.

FA type 1 (FA_1) had a density of 2.42 Mg/m^3 and FA type 2 (FA_2) had a density of 2.35 Mg/m^3. FA_2 was the one employed in the reference mixture, REF2. The main physical properties and the quantities of the traditional mixtures' constituents are listed in Tables 1 and 2, respectively. In the particular case of the grain size fraction 6–14 mm and 14–20 mm, their physical properties were obtained for the larger fraction, namely the grain size fraction 6–20 mm. Subsequently, the characterized grain size fraction 6–20 mm was separated into two aggregates grain size fractions, 6–14 mm and 14–20 mm, for formulating the reference compositions. Figure 1a shows the particle size distribution of the natural aggregates.

Table 1. Specific density of the natural and waste materials used in the concrete formulations.

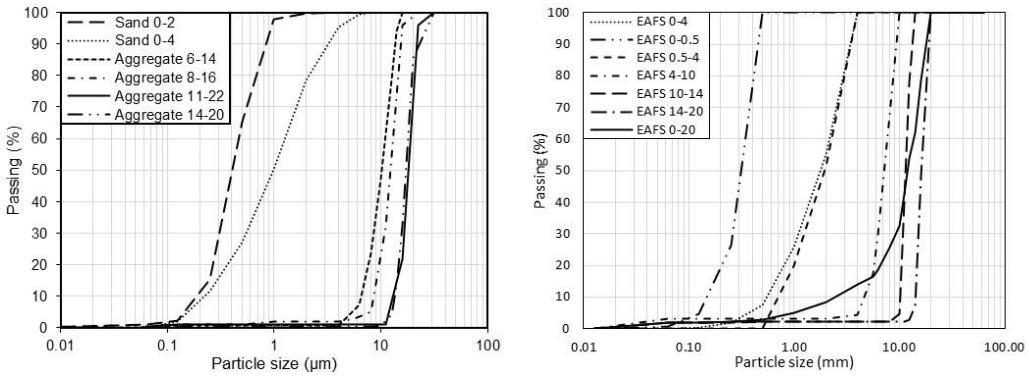
Component	Apparent Particle Density, ρ_a (Mg/m^3)	Particle Density on an Oven-Dried Basis, ρ_{rd} (Mg/m^3)	Particle Density on a Saturated-Dried Basis, ρ_{ssd} (Mg/m^3)	Water Absorption, WA_{24} (%)
SP	—	1.18	—	—
PL	—	1.18	—	—
CEM	—	3.11	—	—
Filler	—	2.70	—	—
FA_1	—	2.42	—	—
FA_2	—	2.35	—	—
Sand 0–2	2.64	2.62	2.63	0.2
Sand 0–4	2.65	2.61	2.63	0.6
Aggregate 6–20	2.70	2.64	2.66	0.8
EAFS 0–4	3.58	3.49	3.51	0.7
EAFS 4–10	3.47	3.25	3.31	2.0
EAFS 10–14	3.40	3.22	3.27	1.6
EAFS 14–20	3.34	3.18	3.22	1.6
EAFS 0–20	3.42	3.25	3.29	1.6

Table 2. Reference mixture compositions, REF1 and REF2 [kg/m^3 or L/m^3].

	REF1	REF2
CEM II/A-L 42.5 R	280	205
FA_2		115
Sand 0–2	415	350
Sand 0–4	495	530
Aggregate 6–14	552	388
Aggregate 14–20	430	580
SP	1.6	1.6
PL	1.4	1.6
Water	165	154.1
w/p	0.54	0.35
w/c	0.59	0.75
% Aggregates	87.11	81.48
% FA	—	9.48

The sustainable concretes were mostly composed of EAFS, obtained from the production of steel in Porto (Portugal). In order to suppress the need for fine aggregates, natural sands with grain sizes of 0–2 mm and/or 0–4 mm were also used. FA_1 or FA_2, and limestone filler were used as fine materials, as well as plasticizer (PL) and superplasticizer (SP). Portland cement CEM II/A-L 42.5 R (CEM) was again used as the binder. The water/powder (w/p) and water/cement (w/c) ratios varied between 0.30–0.55 and 0.54–0.91 (in weight), respectively. EAFS was divided into seven different grain sizes of 0–0.5 mm, 0.5–4 mm, 0–4 mm, 4–10 mm, 10–14 mm, 14–20 mm and 0–20 mm. FA_2 was used in EAFS8C1, EAFS8D1, and FRC_EAFS mixtures. The remaining EAFS mixtures were made using FA_1. The main physical properties of the ingredients EAFS and FA are listed in

Table 1. The physical properties of EAFS grain size fractions 0–0.5 mm, 0.5–4 mm and 0–4 mm were obtained for the larger fraction, namely the grain size fraction 0–4 mm. The characterized grain size fraction 0–4 mm was then separated into the three EAFS grain size fractions for formulating the EAFS concrete compositions.



(**a**) (**b**)

Figure 1. Particle size distribution of the used aggregates: (**a**) natural aggregates; (**b**) EAFS aggregates.

Table 3 shows the estimated elements composition of the EAFS using XRF analysis and the estimated elements composition of FA_1 using XRF, SEM-EDS and XRD analysis. Figure 1b shows the EAFS aggregates particle size distributions with different fractions and Figure 2b shows the appearance of EAFS aggregates with a dimension between 0–20 mm, before its division into fractions. RTSF were provided by the tire production industry in Sines (Portugal) and were added to the EAFS concrete without any initial treatment or preparation. Typically, wastes from tire recycling are subjected to previous screening and cleaning in order to reduce the content of materials other than the steel fibers, for example rubber. However, in this research the viability of using the waste material directly was tested, in order to reduce energy and costs involved in the process. Figure 2a shows the RTSF, where it was possible to identify remains of tire rubber, synthetic fibers and steel fibers of different shapes, lengths and diameters. Table 4 shows the geometric properties of steel fibers. RTSF waste materials containing the steel fibers showed a specific density of 3.42 Mg/m^3.



(**a**) (**b**)

Figure 2. (**a**) representative samples of RTSF; (**b**) EAFS aggregates (0–20 mm) before division into fractions.

Table 3. Element composition of the EAFS and FA by XRF, SEM-EDS and XRD analysis [%].

	EAFS	FA		
	XRF	XRF	EDS	XRD
Al_2O_3	8.91	27.30	28.59	22.1 vitreous *
BaO	0.15			
C			3.65	
CaO	26.73	2.36	1.80	
Cl	0.02			
Cr_2O_3	1.70			
CuO	0.03			
Fe_2O_3	32.33	8.19	6.86	4.8 vitreous *
K_2O	0.23	3.34	1.97	
MgO	4.27	1.42		
MnO	3.25			
Na_2O	0.30	0.99	1.78	
Nb_2O_5	0.02			
P_2O_5	0.51			
SiO_2	20.29	49.12	56.83	28.7 vitreous *
SO_3	0.29	1.30		
SrO	0.04			
TiO_2	0.67	2.32		
V_2O_5	0.14			
WO_3	0.01			
ZnO	0.02			
Other				15.4 vitreous *
Quartz				18.41
Mullite				7.18
Hematite				3.41
Total crystalline phase *				29.00
Total glassy phase				71.00

* Rietveld method.

Table 4. Geometric properties of RTSF.

	Diameter (mm)	Length (mm)	Developed Length (mm)	Slenderness	Curvature Index
Minimum	0.1	5.0	19.0	45.5	0.1
Maximum	1.2	92.0	129.0	651.2	0.9
Mode	0.3	33.0	34.0	225.0	0.3
Average	0.3	33.2	53.3	199.0	0.4
CoV	0.448	0.411	0.358	0.392	0.529

Mix Design of EAFS Structural Concrete

In order to optimize the industrial process of producing EAFS concrete compositions while taking advantage of the least number of fractions, the design procedure was developed using the modified Andreasen and Andersen particle packing method, which reads as follows [32,33]:

$$P(D) = \frac{D^q - D_{min}^q}{D_{max}^q - D_{min}^q} \quad (1)$$

where D is the particle size (μm), $P(D)$ is the fraction of the total solids smaller than size D, D_{max} is the maximum particle size (μm), D_{min} is the minimum particle size (μm), and q is the distribution modulus. The distribution modulus is used to define the ratio between the fine and coarse particles in the mixture, which according to Husken G. [34] can vary between the values of 0.1 for fluid concretes and 0.9 for dense concretes. Studies suggest a q value in the range of 0.35–0.4 for EMC (Earth-Moist Concrete) [34], and of 0.23 for UHPC (Ultra-High Performance Concrete), UHPFRC (Ultra-High Performance Fiber Reinforced Concrete) and UHPHFRC (Ultra-High Performance Hybrid Fiber Reinforced Concrete) [35–39]. For

ULFRC (Ultra-Lightweight Fiber Reinforced Concrete) and for ULC (Ultra-lightweight Concrete) the q values range between 0.32–0.35 [40,41]. In this study the value of q was initially fixed to 0.35. However, in the course of the research, the value of q it has decreased to a minimum value of 0.15. Based on the modified equation of Andreasen and Andersen, Husken G. [32] established an optimized algorithm for optimizing concrete formulations. The algorithm adjusted the proportions of each individual material in the mixture, until an optimum fit between the composed mixture and the target curve was reached. To minimize the deviation between the target curve and the composed mixture the algorithm employed the residual sum of squares (RSS) at defined particle sizes based on the least squares method (LSM), as follows:

$$RSS = \sum_{i=1}^{n} \left(P_{mix}\left(D_i^{i+1}\right) - P_{tar}\left(D_i^{i+1}\right) \right)^2 \quad (2)$$

where P_{mix} is the composed mix and the P_{tar} is the target grading calculated from Equation (2).

With the purpose of reaching an optimal concrete design, this research made use of this algorithm. It should be noted that this algorithm is designed for optimization of the solid skeleton. Other variables such as SP, PL, and the w/p or w/c ratio must be defined by the technician considering the target properties including strength and its balance with the fresh properties. When choosing this methodology, only the solid skeleton formed by the aggregates was considered, the type of SP or PL and the type of fibers were not taken into account. However, some restrictions had to be imposed. Thus, based on the reference mixture REF1, the cement, water and SP amount were fixed in order to start the first iterations of mixtures. PL constituent was not added to the initial EAFS mixtures as it was not considered a relevant admixture. After the first design, using the previously mentioned algorithm with the predefined restrictions and a q value equal to 0.35, it was realized that w/p ratio value would be equal to 0.55. Then, the w/p ratio was kept constant.

Initially, EAFS mixtures based on those predefined variables were made. In the first EAFS mixtures the limestone filler ingredient was considered as an addition. Then, the limestone filler was replaced by the recycled materials EAFS fraction 0–0.5 mm and/or FA. However, depending on the algorithm optimization, the abovementioned fine powders may not be incorporated as ingredients in the new EAFS concrete compositions. For EAFS mixtures based on REF2 the cement, water, SP and PL amounts were changed in accordance with the REF2 values. During the investigation, it was necessary to make some changes to the previously predefined restrictions, in order to obtain EAFS mixtures with the predefined requirements according to the reference mixtures, REF1 and REF2. The restrictions that underwent successive iterations, until the desired EAFS concrete mixture was obtained, were the w/p ratio and the distribution modulus, q. Moreover, the distinct EAFS fractions were combined in different ways. From these different combinations and iterations, several EAFS mixtures emerged, as shown in Tables 5 and 6. These EAFS mixtures present the aggregates amounts as the saturate weight. Figure 3 shows the particle size distribution of the target and resulting grading curves of the selected EAFS mixtures, which were based on the modified Andreasen and Andersen particle packing model.

Finally, 0.5% (in volume) of RTSF was added to the selected EAFS mixture, which was defined as FRC_EAFS (Table 5). The selection of the EAFS mixture was based on the predefined requirements of the reference mixtures REF1 and REF2, by applying the optimized particle packing model, designated as EAFS8D1.

Table 7 shows a summarized description of the abbreviations used to designate the mixtures.

Table 5. Designed EAFS mixtures based on REF1 [kg/m^3 or * L/m^3].

	q = 0.35				q = 0.25		q = 0.20		q = 0.15
EAFS Mixtures	**2**	**3A**	**4**	**6**	**3B**	**8B**	**5C**	**8C**	**8D**
CEM	234	233.7	233.8	233.7	241.5	252.2	254.4	257.4	257.4
FA_1		3.6			123.7	135.5	169.3	210.4	286.5
Filler				22.4					
Sand 0–2	528.3	176.8		66.9	234.7	194.5		225	247.3
Sand 0–4				654.1					
EAFS 0–0.5			316.7				498.2		
EAFS 0.5–4			810.6				879.8		
EAFS 0–4		848.2			792.1	1050.1		832.5	933
EAFS 4–10	734.4	414.4	394.4		363.1		452.5		
EAFS 10–14							144.9		
EAFS 14–20							257.4		
EAFS 0–20	981.8	958	931	1448.5	721.1	978.5		828.4	705.9
* SP	2.61	2.61	2.61	2.61	2.69	2.81	2.84	2.87	2.87
* Water	155.7	151	153.9	158.9	188.5	153.0	199.8	221.5	195.7
w/p [(b)]	0.55	0.55	0.55	0.55	0.48	0.37	0.43	0.45	0.35
w/c	0.67	0.65	0.66	0.68	0.78	0.61	0.79	0.86	0.76
RSS	0.07	0.02	0.02	0.10	0.02	0.03	0.02	0.03	0.03
% EAFS [(a)]	69.2	84.3	91.3	59.7	75.8	77.7	84.0	70.6	67.4
% FA [(a)]		0.1			5.0	5.2	6.4	8.9	11.8

(a) Percentage in weight of solid ingredients. (b) Considers all fine powders with a grain size below 125 µm. * Rietveld method.

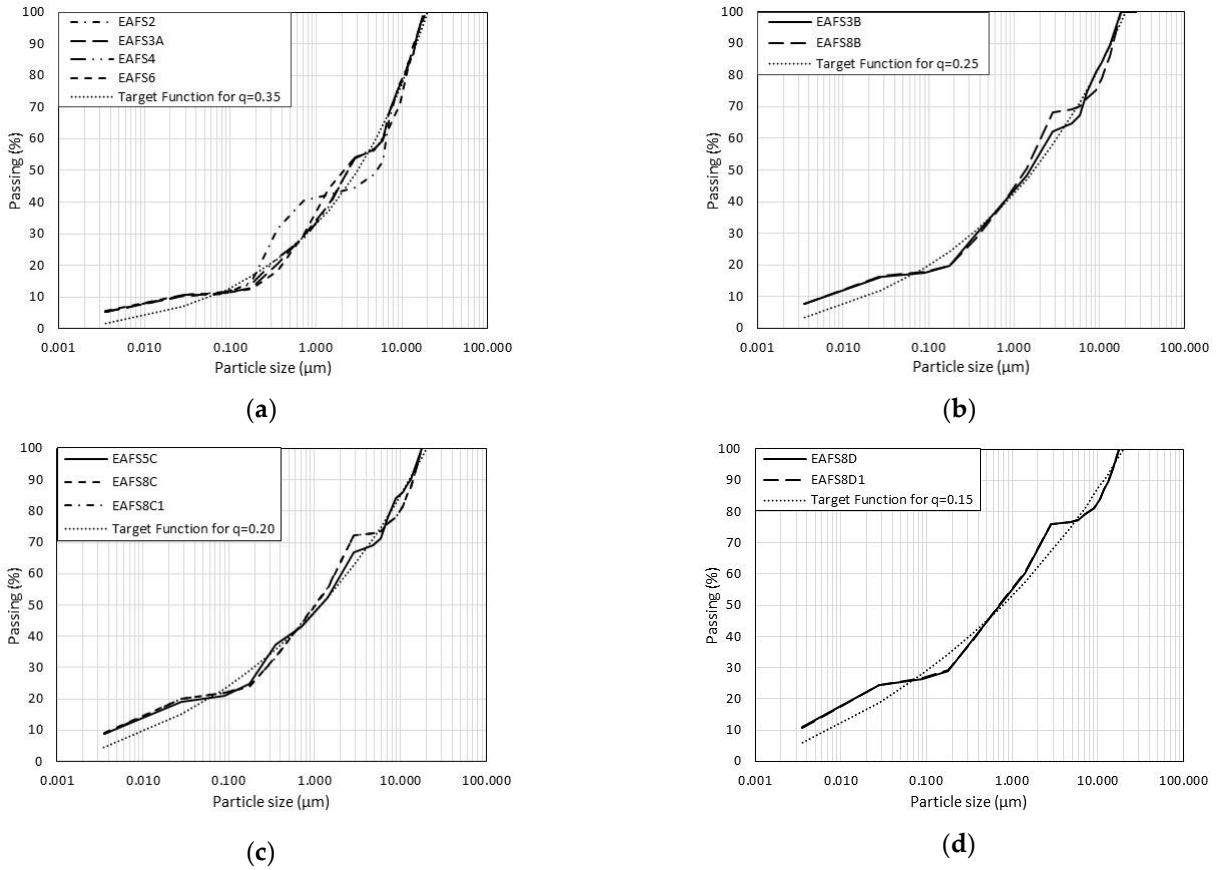


Figure 3. Particle size distribution of the target and resulting grading curves of the EAFS mixtures: (**a**) for q = 0.35; (**b**) For q = 0.25; (**c**) for q = 0.20; (**d**) for q = 0.15.

Table 6. Designed EAFS mixtures based on REF2 [kg/m^3 or * L/m^3].

	q = 0.20	q = 0.15	
EAFS Mixtures	**8C1**	**8D1**	**FRC_EAFS**
CEM	194	209.2	205.8
FA_2	177.1	244	249.5
Sand 0–2	235.9	279.5	288.5
EAFS 0–4	1020.1	979.9	995.4
EAFS 0–20	860.5	764.1	776.4
* SP	1.51	1.63	1.61
* PL	1.51	1.63	1.61
* Water	177.3	165.5	181.33
RTSF			39.3
w/p (b)	0.45	0.35	0.38
w/c	0.91	0.79	0.88
RSS	0.03	0.03	
% EAFS (a)	75.6	70.4	70.4
% FA (a)	7.1	9.9	9.9

(a) Percentage in weight of solid ingredients. (b) Considers all fine powders with a grain size below 125 µm. * Rietveld method.

Table 7. Description of the abbreviations adopted to designate the mixtures performed.

Mixtures	Description
REF1	Reference mixture with a slump class of S3 and a strength class of C30/C37
EAFS2	Mixture based on REF1 with EAFS aggregate size fraction of 4–10 and 0–20 for q = 0.35
EAFS3A	Mixture based on REF1 with EAFS aggregate size fraction of 0–4, 4–10 and 0–20 for q = 0.35
EAFS3B	Mixture based on REF1 with EAFS aggregate size fraction of 0–4, 4–10 and 0–20 for q = 0.25
EAFS4	Mixture based on REF1 with EAFS aggregate size fraction of 0–0.5, 0.5–4, 4–10 and 0–20 for q = 0.35
EAFS5C	Mixture based on REF1 with EAFS aggregate size fraction of 0–0.5, 0.5–4, 4–10, 10–14 and 14–20 for q = 0.25
EAFS6	Mixture based on REF1 with EAFS aggregate size fraction of 0–20 for q = 0.35
EAFS8B	Mixture based on REF1 with EAFS aggregate size fraction of 0–4 and 0–20 for q = 0.25
EAFS8C	Mixture based on REF1 with EAFS aggregate size fraction of 0–4 and 0–20 for q = 0.20
EAFS8D	Mixture based on REF1 with EAFS aggregate size fraction of 0–4 and 0–20 for q = 0.15
REF2	Reference mixture with a slump class of S4 and a strength class of C25/C30
EAFS8C1	Mixture based on REF2 with EAFS aggregate size fraction of 0–4 and 0–20 for q = 0.20 (low cement amount)
EAFS8D1	Mixture based on REF2 with EAFS aggregate size fraction of 0–4 and 0–20 for q = 0.15 (low cement amount)
FRC_EAFS	EAFS8D1 mixture with the incorporation of RTSF

2.2. Mixing Procedure

As a first step, it was necessary to determine the moisture content of the aggregates by drying them in accordance with [42]. Then, it was possible to calculate the amount of water required to saturate the aggregates and the amount of intrinsic water (water inside the aggregate pores). Therefore, the total water of the mixture was obtained by taking also into account the water necessary to saturate the aggregates.

The mixing was carried out in a horizontal mixer with a maximum capacity of 90 liters. The procedure was adapted during the study, in order to consider the particularly porous and glassy nature of EAFS, which leads to the gradual absorption of water during mixing.

Before the mixing process was started the mixer was moistened, so that it would not absorb part of the mixing water. After this, the mixing process was started, where the mixture constituents were added in phases. Initially, the aggregates (coarse and fine) were added in a decreasing diameter sequence, and then the water required to saturate the aggregates (approximately 1/3 of the total water of the mixture) was added. Mixing was carried out for 3 min more, until the aggregates were saturated, and the mixture was homogeneous. The fine materials and additions were then added to the mixer, and the remaining water and admixtures were added continuously for about 3 min with the mixer running. The mixing process was then allowed to continue for an additional period of 5 min.

Regarding the mix with the incorportion of recycled fibers, these were added after the 5 min period of mixing mentioned above, with subsequent mixing until a good fiber distribution was obtained, which occured approximately 5 min later.

2.3. Specimen Preparation

For each mixture, twelve cylindrical specimens with a diameter of 150 mm and a height of 300 mm were used [43]. For each age (7, 28 and 90 days) four specimens were tested, to assess the mechanical properties of the concrete in terms of uniaxial compression strength and elasticity modulus. In order to characterize the physical properties, namely the water absorption by immersion at vacuum and the air and water permeability, six cylindric specimens with a diameter of 50 mm and 40 mm thick were extracted from a slab ($300 \times 300 \times 60$ mm^3) that was cast from each mixture. For water absorption characterization by immesion at atmospheric pressure and by capillarity, and for carbonation resistance characterization, three cubic specimens with a 100 mm edge, three cylindric specimens with a diameter of 150 mm and a height of 300 mm and six rectangular prisms with a 100 mm edge and 400 mm length of each mixture were cast. The entire vibration and casting process followed the EN 12390-2 recommendations [44]. After 24 h of curing the specimens were demolded and kept in a climatic room that guaranteed constant temperature, t, of 20 ± 2 °C and relative humidity, RH, of 60 ± 5%, until testing. In the case of the rectangular prisms ($400 \times 100 \times 100$ mm^3) the curing conditions were t of 20 ± 2 °C and RH of 95 ± 5% for 28 days, and after that, the specimens were kept in the laboratory (t between 18–25 °C and RH between 50–65%) for 14 days more. The slabs ($300 \times 300 \times 60$ mm^3) were immersed in water at a temperature of 20 ± 2 °C. The specimens used for mechanical characterization were rectified before testing. Table 8 shows the experimental program of the tests performed, type and number of specimens and the corresponding followed standards for each of the different concrete mixtures studied.

2.4. Testing Procedures

2.4.1. Fresh Properties

According to the European Standard EN 12350-2 [45] the Abrams cone can be used to indirectly evaluate the viscosity and the shear stress of the mixtures in the fresh state. In this research this was the procedure adopted to characterize workability of each composition.

2.4.2. Mechanical Properties

The uniaxial compression tests were aimed at obtaining the compressive strength and elasticity modulus, according to the standards EN 12390-13 [46] and EN 12390-3 [47], respectively. These were carried out under closed-loop displacement control, at a displacement rate of 0.005 mm/s and using an actuator with a 1600 kN load cell. The adopted procedure consisted first of determining the compressive strength in one specimen at each age. Thus, based on this estimated value, the loading procedure to determine the elasticity modulus in the three remaining specimens could be established. After obtaining specimens' elasticity modulus, the uniaxial compression test was performed until failure to obtain the stress—strain relationship. The tests were performed using four LVDTs (Linear Variable Differential Transducers), one external LVDT and three internal LVDTs, located between plates in the sample (Figure 4a). The external LVDT was used just for confirmation purposes. The

three internal LVDTs were used to determine the mean value of the axial displacement in each specimen and defining the compressive stress—strain curves. Figure 4b shows the set-up adopted for the elasticity modulus characterization.

Table 8. Summarized scheme of the overall tests performed for each type of concrete mixture.

Characterization Type	Tests	Specimen Type	N° of Specimens	Standards
Fresh properties	Slump	—	—	EN 12350-2
Mechanical properties	Uniaxial compression	Cylinder (ϕ = 150 mm; H = 300 mm)	12	EN 12390-13
	Elasticity modulus	Cylinder (ϕ = 150 mm; H = 300 mm)	9	EN 12390-3
Physical properties	Water absorption by immersion at atmospheric pressure	Cubic (100 × 100 × 100 mm)	3	LNEC E 394 based on the RILEM Recommendation CPC11.1
	Water absorption by immersion at vacuum	Cylinder (ϕ = 50 mm; H = 40 mm)	6	LNEC E 395 based on the RILEM Recommendation CPC11.3
	Water absorption by capillarity	Cylinder (ϕ = 150 mm; H = 300 mm)	3	LNEC E 393 RILEM Recommendation CPC11.2
	Air and water permeability	Cylinder (ϕ = 50 mm; H = 40 mm)	6	Leeds Permeability Cell (LPC) developed at Leeds University
	Accelerated carbonation	Rectangular prism (100 × 100 × 400 mm)	6	BS 1881-210

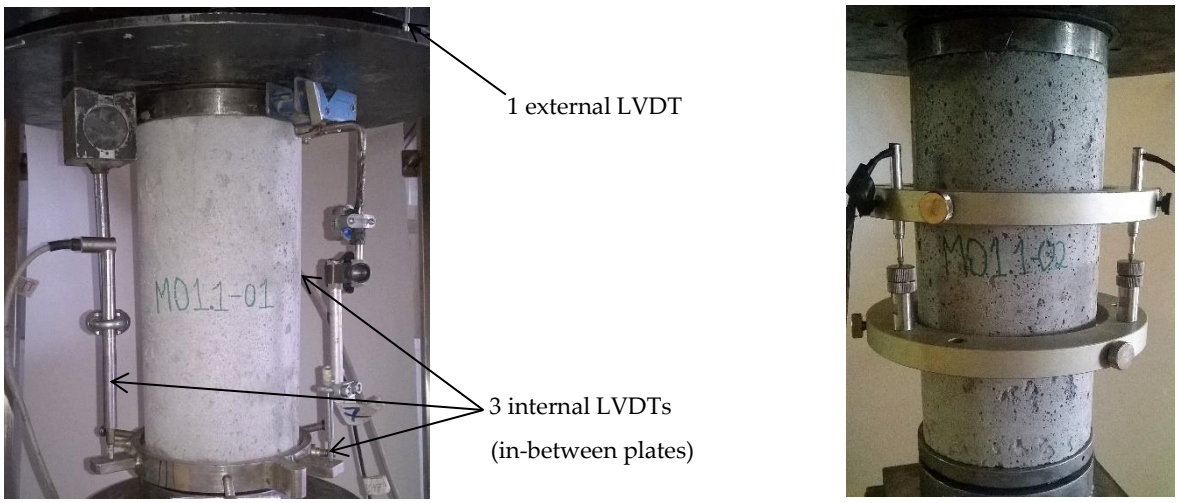


Figure 4. Experimental set-up: (**a**) uniaxial compression test; (**b**) elasticity modulus.

2.4.3. Physical Properties

Physical tests were performed at 28 days after casting for REF2, EAFS8D1 and FRC_EAFS mixtures. It was considered appropriate to carry out these tests only for the reference mixture REF2 as baseline, considering that it contains less cement and may be more likely to perform worse in terms of durability. These tests were focused on the determination of water absorption by immersion, at atmospheric pressure and at vacuum,

and by capillarity. Permeability to air and water, as well as resistance to carbonation were characterized as well. The water absorption by immersion, at atmospheric pressure and at vacuum, and by capillarity, followed the Portuguese Specifications LNEC E 394 [48], LNEC E 395 [49] and LNEC E 393 [50], respectively, which are based on the RILEM Recommendation CPC11.1, CPC11.3 and CPC11.2 [51–53]. The air and water permeability tests were performed using the Leeds Permeability Cell (LPC) developed at Leeds University [54]. This permeameter ensures that the specimens are subjected to a stable and uniaxial flow state, and that the fluid passes through the samples under a certain pressure for a desired period of time (Figure 5). In these tests, the six cylindrical specimens used previously for water absorption tests by immersion at vacuum were reused. After the water absorption test by immersion at vacuum, the specimens were dried in a ventilated oven at a temperature of 105 ± 5 °C until the mass difference measured during a 24 h period was less than 0.1%. Later, the specimens were waterproofed laterally, with a thin layer of silicone, in order to ensure uniaxial penetration and transport through the tops of the specimens. After 12 h to allow the drying of the silicone, the specimens were placed in the LPC to carry out the air and water permeability tests, following this sequence and always keeping the specimen inside the LPC. The carbonation resistance was assessed by accelerated carbonation tests following the standard BS 1881-210 [55]. For this, before placing the specimens in the carbonatation storage chamber, their upper, lower and two end faces were sealed. Thus, following the guidelines of the standard, only the lateral faces of the specimens were exposed to carbonation environment.



(**a**) (**b**)

Figure 5. Air and water permeability test set-up: (**a**) Leeds Permeability Cell (LPC); (**b**) specimens used.

3. Results

3.1. Fresh Properties

For an initial assessment the Abrams cone was used to characterize the fresh state behavior of the mixtures with the slump tests. Table 9 shows the results obtained for the REF1, REF2 and EAFS mixtures, with and without RTSF.

Table 9. Results of the fresh properties reached for the reference mixtures REF1 and REF2 and for the EAFS mixtures.

q	Mixtures	Slump (mm)	Slump Class
	REF1	110	S3
0.35	EAFS6	30	S1
	EAFS2	164	S4
	EAFS3A	10	S1
	EAFS4	0	S1
0.25	EAFS8B	20	S1
	EAFS3B	40	S1
0.20	EAFS8C	80	S2
	EAFS5C	120	S3

Table 9. *Cont.*

q	Mixtures	Slump (mm)	Slump Class
0.15	EAFS8D	125	S3
	REF2	160	S4
0.20	EAFS8C1	50	S1
0.15	EAFS8D1	160	S4
	FRC_EAFS	0	S1

3.2. Mechanical Properties

Compressive Strength

Table 10 shows the results obtained for the elasticity modulus, $E_{cm,t}$ at 7, 28 and 90 days, and for the uniaxial compression tests. The later include the characteristic compressive strength at 28 days after casting, f_{ck} and the average compressive strength at 7, 28 and 90 days after casting, $f_{cm,t}$. Equations (3) and (4) were used to obtained the characteristic compressive strengths, f_{ck}, according to the Standard NP EN 206-1 [56]. The coefficients of variation obtained for both the elasticity modulus and the average compressive strength, were quite low, in the ranges of 0.01–0.25 and 0.00–0.43, respectively:

$$f_{cm} \geq f_{ck} + 4 \quad (3)$$

With:

$$f_{ci} \geq f_{ck} + 2 \quad (4)$$

Table 10. Results of the mechanical properties obtained for the REF1, REF2 and EAFS mixtures.

q	Mixtures	f_{cm} (MPa)			f_{ck} (MPa)	Strength Class	E_{cm} (GPa)		
		7 Days	28 Days	90 Days			7 Days	28 Days	90 Days
	REF1	22.70	30.68	30.40	26.68	C25/30	24.63	27.44	30.80
0.35	EAFS6	12.86	17.54	18.09	13.54	C12/15	24.79	24.58	26.49
	EAFS2	12.38	19.43	23.35	15.43	C12/15	26.22	30.47	31.31
	EAFS3A	10.29	—	—	—	—	18.76	—	—
	EAFS4	10.61	9.43	13.17	6.59	—	25.44	22.11	31.15
0.25	EAFS8B	25.20	36.17	—	33.01	C30/37	34.02	37.97	—
	EAFS3B	18.60	26.29	—	22.29	C20/25	30.62	35.01	—
0.20	EAFS8C	20.88	35.14	—	31.14	C30/37	32.43	35.79	—
	EAFS5C	22.02	34.91	—	30.91	C30/37	31.78	35.25	—
0.15	EAFS8D	22.66	35.66	—	31.66	C30/37	34.90	35.37	—
	REF2	18.40	27.37	35.85	24.10	C20/25	24.58	27.01	30.14
0.20	EAFS8C1	17.87	31.14	39.93	27.14	C25/30	32.76	37.95	39.91
0.15	EAFS8D1	15.40	29.22	36.82	25.22	C25/30	29.70	36.04	36.82
	FRC_EAFS	13.60	25.09	31.64	21.09	C20/25	30.07	37.37	36.74

3.3. Physical Properties

3.3.1. Water Absorption by Immersion

The water absorption test by immersion at atmospheric pressure was performed taking into consideration three different weight measurements: dry mass (M_d), saturated mass (M_s), and hydrostatic mass (M_h). For each composition, the three specimens were dried in a ventilated oven at a temperature of 105 ± 5 °C until the difference in mass in a 24 h time interval was below 0.1%. Later, the specimens were immersed in water until the change in mass in a 24 h time interval was below 0.1%, and subsequently the hydrostatic mass was

measured. The water absorption by immersion at atmospheric pressure (W_i) was calculated using the following equation according to the standard LNEC E 394 [48]:

$$W_i = \frac{(M_s - M_d)}{(M_s - M_h)} \times 100 \quad (5)$$

For water absorption by immersion under vacuum, three different weight measurements were obtained: dry mass (M_d), saturated mass after water absorption under vacuum (M_s), and hydrostatic mass (M_h). The test consisted of dying the specimens in a ventilated oven at a temperature of 105 ± 5 °C until the mass variation for a 24 h time interval was below 0.1%. The specimens were then subjected to a vacuum pressure of 1 bar for 24 h and water was subsequently introduced slowly, in such a way that the specimens were completely submerged. The vacuum was maintained for an additional 24 h period. The pressure was then released to atmospheric level and the specimens remained submerged for 24 h to ensure full saturation. Lastly, the hydrostatic mass was obtained. The water absorption by immersion under vacuum (W_{vc}) was calculated using the following equation according to the Standard LNEC E 395 [49]:

$$W_{vc} = \frac{(M_s - M_d)}{(M_s - M_h)} \times 100 \quad (6)$$

Tables 11 and 12 show the results of water absorption by immersion at atmospheric pressure and under vacuum, respectively. It should be noted that $W_{i,m}$ and $W_{vc,m}$ are the average values corresponding to water absorption by immersion at atmospheric pressure and by immersion under vacuum, respectively. Figure 6 shows the test set-up for both water absorption by immersion at atmospheric pressure, and under vacuum.



(**a**) (**b**)

Figure 6. Set-up of water absorption test by immersion: (**a**) at atmospheric pressure; (**b**) under vacuum.

Table 11. Results of water absorption test by immersion at atmospheric pressure for the REF2 mixture and for the mixtures with EAFS and RTSF.

Specimen	M_d (g)	M_s (g)	M_h (g)	W_i (%)	W_{im} (%)	CoV
REF2_P1	2234.8	2355.9	1322.3	11.72		
REF2_P2	2237.0	2359.7	1325.5	11.87	11.56	0.028
REF2_P3	2278.2	2394.1	1350.7	11.11		
EAFS8D1_P1	2646.7	2798.2	1755.0	14.53		
EAFS8D1_P2	2690.6	2840.6	1788.0	14.25	14.47	0.011
EAFS8D1_P3	2666.7	2821.1	1765.0	14.62		
FRC_EAFS_P1	2593.5	2762.4	1717.5	16.16		
FRC_EAFS_P2	2566.2	2736.1	1695.2	16.32	16.22	0.005
FRC_EAFS_P3	2587.5	2756.4	1711.7	16.17		

Table 12. Results of water absorption test by immersion under vacuum for the for the EAFS8D1 mixture.

Specimen	M_d (g)	M_s (g)	M_h (g)	W_{vc} (%)	W_{vcm} (%)	CoV
EAFS8D1_C1	160.75	174.18	111.08	21.28	21.75	0.020
EAFS8D1_C2	160.81	174.56	110.35	21.41		
EAFS8D1_C3	159.39	173.07	109.39	21.48		
EAFS8D1_C4	156.96	171.40	107.65	22.65		
EAFS8D1_C5	159.36	173.20	109.32	21.67		
EAFS8D1_C6	154.43	168.14	105.86	22.00		

3.3.2. Water Absorption by Capillarity

The water absorption by capillarity test, also called the sorptivity test, was performed first by drying the specimens in a ventilated oven at a temperature of 105 ± 5 °C until the mass variation during 24 h was lower than 0.1%. Later, the specimens were immersed in water at a height of 5 ± 1 mm of water, for 72 h, during which the increase in mass of the specimens was measured. The water absorption by capillarity (W_c) was determined by the ratio between the increase in weight, $M_i - M_o$, and the cross-section of the bottom surface of the specimen (Ω_i), i.e., the surface area in contact with the water, according to the following equation [50]:

$$W_c = \frac{(M_i - M_0)}{\Omega_i} \times 100 \quad (7)$$

where M_i is the mass of the specimen in contact with the water for different times of reading ($\sqrt{t_i}$), and M_0 is the dry mass of the specimen. Tables 13–15 show the results of water absorption by capillarity for the reference mixture REF2, and for the designed mixtures EAFS8D1 and FRC_EAFS, respectively. Figure 7 shows the specimens during the water absorption by capillarity test.

Table 13. Results of water absorption tests by capillarity obtained for the reference mixture REF2.

Time ($min^{0.5}$)	Absorption Mass ($\times 10^3$ mg)			W_c (mg/mm^2)			W_{cm} (mg/mm^2)
	C1	C2	C3	C1	C2	C3	
0.00	11,676.7	11,659.9	11,669.48	0.000	0.000	0.000	0.000
7.75	11,688.02	11,669.92	11,682.42	0.658	0.585	0.752	0.665
10.95	11,689.94	11,671.98	11,684.76	0.770	0.705	0.888	0.788
13.42	11,696.3	11,674.84	11,688.14	1.139	0.872	1.085	1.032
15.49	11,696.3	11,678.32	11,691.74	1.139	1.076	1.294	1.170
17.32	11,698.52	11,680.34	11,694.12	1.268	1.194	1.432	1.298
34.64	11,718.84	11,701.12	11,716.7	2.450	2.407	2.745	2.534
36.33	11,720.82	11,702.44	11,718.02	2.565	2.484	2.822	2.623
37.95	11,722.36	11,703.76	11,719.74	2.654	2.561	2.922	2.712
39.50	11,723.88	11,705.2	11,721.82	2.742	2.645	3.042	2.810
40.99	11,725.6	11,706.9	11,723.16	2.842	2.744	3.120	2.902
51.38	11,736.38	11,717.72	11,735.5	3.469	3.376	3.838	3.561
52.54	11,736.64	11,717.8	11,735.82	3.484	3.381	3.856	3.574
53.67	11,738.86	11,719.1	11,737.08	3.613	3.457	3.929	3.666
54.77	11,739.68	11,720.2	11,738.46	3.661	3.521	4.010	3.731
55.86	11,740.8	11,721.3	11,739.62	3.726	3.585	4.077	3.796
63.87	11,748.54	11,729.1	11,748.28	4.176	4.041	4.581	4.266
64.81	11,748.8	11,729	11,749.1	4.191	4.035	4.628	4.285
65.73	11,749.84	11,729.6	11,749.36	4.251	4.070	4.643	4.322
67.53	11,751.76	11,731.2	11,751.36	4.363	4.163	4.760	4.429
74.30	11,757.22	11,736.64	11,757.78	4.680	4.481	5.133	4.765
75.89	11,758.22	11,737.64	11,758.64	4.739	4.539	5.183	4.820
77.46	11,759.08	11,738.56	11,759.74	4.789	4.593	5.247	4.876

Table 14. Results of water absorption tests by capillarity for the EAFS8D1 mixture.

Time ($min^{0.5}$)	Absorption Mass ($\times 10^3$ mg)			W_c (mg/mm^2)			W_{cm} (mg/mm^2)
	C1	C2	C3	C1	C2	C3	
0.00	15,513.04	15,462.02	15,443.78	0.00	0.00	0.00	0.00
7.75	15,522.58	15,471.74	15,452.7	1.34	1.42	1.34	1.37
10.95	15,530.22	15,479.26	15,458.8	1.87	1.97	1.84	1.89
13.42	15,536.04	15,485.84	15,465.48	2.30	2.39	2.18	2.29
15.49	15,541.16	15,491.28	15,470.76	2.62	2.76	2.56	2.65
17.32	15,545.3	15,495.68	15,474.46	2.91	3.07	2.85	2.94
34.64	15,592.54	15,544.06	15,519.78	3.14	3.31	3.06	3.17
36.33	15,596.04	15,547.44	15,522.9	5.78	6.03	5.60	5.80
37.95	15,599.12	15,550.54	15,525.96	5.97	6.22	5.77	5.99
39.50	15,601.96	15,553.3	15,528.46	6.14	6.40	5.94	6.16
40.99	15,604.54	15,556.1	15,530.78	6.30	6.55	6.08	6.31
51.38	15,629.54	15,580.64	15,553.42	6.45	6.71	6.21	6.46
52.54	15,631.36	15,582.72	15,555.38	7.84	8.09	7.48	7.81
53.67	15,633.16	15,584.64	15,556.94	7.94	8.21	7.59	7.91
54.77	15,635.18	15,586.5	15,558.7	8.04	8.32	7.68	8.01
55.86	15,637.16	15,588.12	15,560.26	8.16	8.42	7.78	8.12
63.87	15,654.38	15,606.02	15,576.56	8.27	8.51	7.87	8.21
64.81	15,655.98	15,607.5	15,578.1	9.23	9.52	8.78	9.18
65.73	15,657.3	15,608.8	15,579.4	9.32	9.60	8.87	9.26
67.53	15,660.7	15,612.1	15,582.66	9.39	9.67	8.94	9.33
74.30	15,673.64	15,625.1	15,594.98	9.58	9.86	9.12	9.52
75.89	15,676.36	15,627.92	15,598.04	10.30	10.59	9.81	10.24
77.46	15,678.88	15,630.22	15,600.12	10.46	10.75	9.98	10.40

Table 15. Results of water absorption tests by capillarity for the FRC_EAFS mixture.

Time ($min^{0.5}$)	Absorption Mass ($\times 10^3$ mg)			W_c (mg/mm^2)			W_{cm} (mg/mm^2)
	C1	C2	C3	C1	C2	C3	
0.00	13,386.32	13,406.08	13,308.64	0.00	0.00	0.00	0.00
7.75	13,402.76	13,419.58	13,325.06	0.94	0.78	0.96	0.90
10.95	13,407.16	13,423.16	13,329.14	1.20	0.99	1.20	1.13
13.42	13,412.06	13,427.1	13,332.96	1.48	1.22	1.43	1.37
15.49	13,417.9	13,432.06	13,338.44	1.81	1.51	1.75	1.69
17.32	13,421.28	13,435.36	13,341.88	2.00	1.70	1.95	1.89
34.64	13,461.02	13,466.16	13,376.86	4.28	3.49	4.00	3.93
36.33	13,463.92	13,468.1	13,379.52	4.45	3.61	4.16	4.07
37.95	13,466.78	13,471.1	13,382.76	4.61	3.78	4.35	4.25
39.50	13,470.4	13,473.68	13,385.56	4.82	3.93	4.51	4.42
40.99	13,473.26	13,476.32	13,387.98	4.99	4.08	4.65	4.57
51.38	13,494.86	13,493.92	13,407.46	6.22	5.11	5.80	5.71
52.54	13,496.48	13,494.64	13,408.48	6.32	5.15	5.86	5.77
53.67	13,499.24	13,496.72	13,410.8	6.48	5.27	5.99	5.91
54.77	13,501.32	13,498.38	13,412.74	6.60	5.37	6.11	6.02
55.86	13,503.5	13,500.18	13,415.08	6.72	5.47	6.24	6.14
63.87	13,519.2	13,513.22	13,429.3	7.62	6.23	7.08	6.98
64.81	13,521.12	13,514.28	13,430.72	7.73	6.29	7.16	7.06
65.73	13,522.64	13,515.7	13,432.1	7.82	6.37	7.24	7.14
67.53	13,525.8	13,518.1	13,434.96	8.00	6.51	7.41	7.31
74.30	13,538.6	13,527.84	13,446.26	8.73	7.08	8.07	7.96
75.89	13,540.94	13,529.48	13,448.34	8.87	7.17	8.19	8.08
77.46	13,543.32	13,531.04	13,450.64	9.00	7.26	8.33	8.20



(**a**) (**b**)

Figure 7. (**a**) Set-up for water absorption test by capillarity; (**b**) representative specimens after a certain time of exposure to water, during the absorption test by capillarity.

3.3.3. Permeability to Air and Water

For air and water absorption, two different coefficients were obtained. In case of air permeability, the modified D'Arcy's law used for gases was applied according to the following equation:

$$K_G = \frac{2v \cdot \eta \cdot L \cdot P_2}{A\left(P_1^2 - P_2^2\right)} \quad (8)$$

where K_G is the coefficient of gas permeability, v is the gas flow, η is the dynamic viscosity of the gas (considered as 18.2×10^{-6} Ns/m^2), L is the thickness of the concrete cross-section, A, is the concrete cross-section traveled by the gas, P_1 is the absolute inlet gas pressure (in the current case 3 bar) and P_2 is the absolute outlet gas pressure (atmospheric pressure, 1 bar). In order to measure the gas flow, v, five constant flow readings were taken by measuring the travel time of a soap bubble for a known distance of 10 cm (T_{10}). For this purpose, a pipette with an inner diameter of 2.5 mm was used. For the determined water permeability coefficient, k_W, the *Valenta* equation was employed (Equation (9)):

$$k_w = \frac{W_{vc} \times {d_p}^2}{2 \times t \times h} \quad (9)$$

where W_{vc} is the porosity of the specimen (determined above), d_p is the water penetration depth, t is the time during which the pressure was applied, i.e., the time taken to reach a penetration depth x_d (adopted as 3 h), and h is the equivalent pressure to the water head (adopted 3 bar = 30.621 mH_2O). In order to measure the depth of water penetration, d_p, eight readings were taken on each of the two broken faces of the specimen obtained after splitting tensile test. To improve the readings, a color indicator—phenolphthalein—was used, in combination with the water, which evidences the boundary of water penetration. The conversion factor for the coefficient, k_W, when using phenolphthalein solution, from m/s to m^2, is: K_W (m^2) = 1.3×10^{-7} k_W (m/s). Tables 16 and 17 show the results of permeability to air and water obtained for EAFS8D1 mixture, including the gas and water coefficients (K_G and K_W), the average specimen length (L_m), cross-section area (A_m), travel time of a soap bubble for a distance of 10 cm (T_{10m}) and depth of water penetration (d_{pm}). The coefficients of variation obtained for the parameters analyzed were somewhat high, which is normal due to the heterogeneity of the porous structure. Figure 8 shows a representative EAFS8D1 specimen where water penetration was measured after performing the water permeability test in LPC.

Table 16. Results of air permeability obtained for EAFS8D1 mixture.

Specimen	L_m (mm)	A_m (mm^2)	T_{10m} (s)	v ($\times 10^{-8}$ m^3/s)	K_G ($\times 10^{-16}$ m^2)	K_{Gm} ($\times 10^{-16}$ m^2)	CoV
EAFS8D1_C1	39.13	1640.66	9.279	5.290	0.584	0.558	0.07
EAFS8D1_C2	39.02	1649.10	10.082	4.869	0.533		
EAFS8D1_C3	39.15	1642.63	9.060	5.418	0.597		
EAFS8D1_C4	39.37	1642.63	9.036	5.432	0.602		
EAFS8D1_C5	39.38	1640.30	10.635	4.616	0.513		
EAFS8D1_C6	38.45	1634.56	10.274	4.778	0.520		

Table 17. Results of water permeability obtained for EAFS8D1 mixture.

Specimen	d_{pm} (mm)	K_W ($\times 10^{-18}$ m^2)	K_{Wm} ($\times 10^{-18}$ m^2)	CoV
EAFS8D1_C1	9.47	3.751	4.20	0.40
EAFS8D1_C2	10.82	4.929		
EAFS8D1_C3	11.57	5.646		
EAFS8D1_C4	11.96	6.366		
EAFS8D1_C5	8.84	3.324		
EAFS8D1_C6	5.29	1.210		



Figure 8. Representative EAFS8D1 specimens after water permeability test.

3.3.4. Resistance to Carbonation

Carbonation resistance was measured using an accelerated carbonation test. The specimens were exposed to an environment with a concentration of 5 ± 0.5% of carbon dioxide at a temperature of 20 ± 2 °C and relative humidity of 55 ± 5% for up to 186 days. For each of the exposure times adopted, as shown in Table 18, the failure surfaces obtained after splitting the beam specimens into two halves were sprayed with a phenolphthalein solution, resulting in a pink coloration showing the uncarbonated concrete portion. As shown in Table 17, this color difference was used to measure the carbonation depth. The carbonation resistance, R_{c65}, was calculated using equation (10), following the recommendation of the Portuguese Standard LNEC E 465 [57]):

$$R_{c65} = \frac{2 \times C_{acel} \times t_1}{X_1^2} \quad (10)$$

where C_{acel} is the CO_2 concentration adopted to accelerate the carbonation process (=90 × 10^{-3} kg/m^3), and t_1 is the time required to reach a carbonation depth X_1 in the specimen. The obtained variables of carbonation resistance (R_{c65}), average carbonation resistance (R_{c65m}), time (t_1) and average carbonation depth (X_{1m}) for REF2, EAFS8D1 and FRC_EAFS mixtures are shown in Tables 19 and 20.

Table 18. Evolution of carbonation depth at increasing exposure times for the REF2 mixture and for the mixtures designed with EAFS and RTSF.

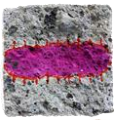
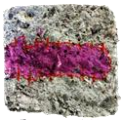
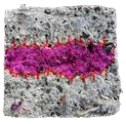
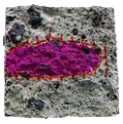
t_1 (Days)	REF2	EAFS8D1	FRC_EAFS
28			
56			
70			
90			
122			
143			
149			
163			
170			
174			
186			

Table 19. Results of average carbonation depth, X_{1m}, for the REF2 mixture and for the mixtures designed with EAFS and RTSF.

t_1 (Days)	X_{1m} (mm)		
	REF2	**EAFS8D1**	**FRC_EAFS**
28	19.12	15.41	17.07
56	27.22	20.63	23.17
63	27.85	22.26	22.80
70	28.70	24.89	23.44
90	28.83	24.67	24.61
122	34.11	28.79	28.97
143	38.10	32.10	33.15
149	38.36	32.69	34.83
163	41.31	35.72	34.61
170	43.71	36.13	36.24
174	43.19	36.29	35.64
186	42.29	37.00	35.83

Table 20. Results of carbonation resistance, R_{c65}, for the REF2 mixture and for the mixtures designed with EAFS and RTSF.

t_1 (Days)	R_{c65} (kg·year/m^5)			R_{c65m} (kg·year/m^5)/CoV		
	REF2	**EAFS8D1**	**FRC_EAFS**	**REF2**	**EAFS8D1**	**FRC_EAFS**
28	37.75	58.17	47.39	48.92/0.189	65.30/0.076	63.42/0.119
56	75.51	64.92	51.44			
63	40.06	62.69	59.75			
70	41.92	55.73	62.82			
90	53.39	72.93	73.27			
122	51.70	72.59	71.69			
143	48.58	68.45	64.19			
149	49.94	68.74	60.58			
163	47.10	62.99	67.10			
170	43.87	64.22	63.85			
174	45.99	65.15	67.54			
186	51.28	67.01	71.46			

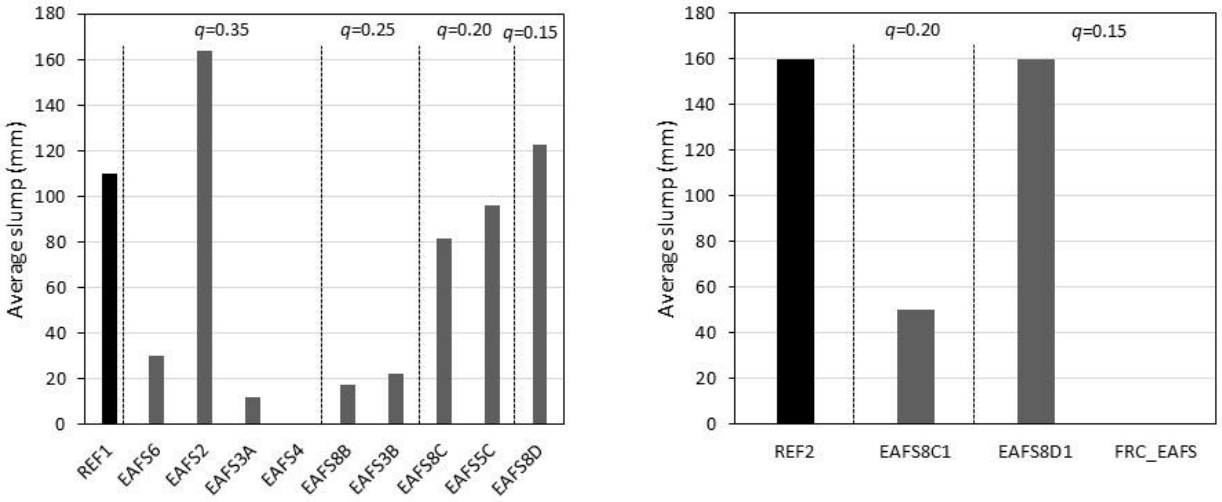
4. Discussion

4.1. Fresh Behavior

The EAFS aggregates significantly altered concrete fresh state behavior when compared to natural aggregates typically used in structural concrete design. This is most likely due to the increased water absorption by the EAFS aggregates and the lack of fine particles which may be clearly identified in the grading curves (Figure 1b). Compositions have been shown to be very sensitive to the process of mixing and to the w/p or w/c ratio, most likely due to the porous nature of the EAFS aggregates. The EAFS aggregates porosity leads to the gradual absorption of water during the mixing process, resulting in alterations of the fresh and hardened behavior. In this regard, it is important to adapt the mixing process in order to take the best advantage of the physical properties of EAFS aggregates. This problem extends to any other situation where alternative aggregates or ingredients are included in conventional concrete mixtures, mainly in the case of the incorporation of wastes or industrial by-products.

As shown in Figure 9, EAFS concrete mixtures showed distinct behaviors, initially very different from REF1 and REF2. Figure 10 shows some of the results obtained for representative specimens during the slump test. The mixtures EAFS3A and 4 (Figure 10c), with a distribution modulus of 0.35, had a very dry behavior; therefore, it was decided to decrease the distribution modulus in the subsequent mixtures. It seems that the porous nature of EAFS requires a greater volumetric percentage of paste in the concrete, necessary

to cover the pores at the surface of the EAFS aggregates and lubricate the interparticle movement, in order to reach equivalent fresh behaviors. With the change from q = 0.35 to q = 0.25, the fluid behavior did not show great improvement, although workability seemed to show an improvement. With the decrease in the distribution modulus to 0.20 and 0.15, a remarkable improvement in fluidity was observed, giving these mixtures the best performance in terms of fresh behavior (Figure 10d,e), with the exception of EAFS2. EAFS2 was the only alternative mixture with q = 0.35 that showed a fresh behavior close to the expected one. This may be explained by the fact that the optimization procedure, in this case, resulted in a greater amount of fine sand, probably because the aggregate fractions selected generated an unbalance in the grading curve, that ended up being fully compensated with fine sand. The mixture EAFS8D1 has demonstrated a good workability and was very close to the one observed in reference mixture REF2, proving that the use of q = 0.15, in the Andreasen and Andersen model, was adequate. Furthermore, the addition of fibers in fresh state caused a loss of workability, resulting in a FRC slump equal to zero. Thus, the FRC_EAFS was characterized as a dense concrete.



(**a**) (**b**)

Figure 9. Results of average slump: (**a**) for REF1 and mixtures designed with EAFS; (**b**) for REF2 and mixtures designed with EAFS.



(**a**) (**b**) (**c**)

Figure 10. *Cont.*



(**d**) (**e**)

Figure 10. Images of representative specimens during slump test of REF and EAFS mixtures: (**a**) REF1 mixture with a slump class S3; (**b**) REF2 mixture with a slump class S4; (**c**) EAFS mixture with a slump class S1; (**d**) EAFS mixture with a slump class S2/S3; (**e**) EAFS mixture with a slump class S4.

4.2. Mechanical Properties

4.2.1. Compressive Behavior of EAFS Mixtures

The average compressive strength, f_{cm}, and the average elasticity modulus, E_{cm}, obtained when considering REF1 as the reference mixture are presented in Figure 11. The same results but considering REF2 as the reference mixture are presented in Figure 12. The failure modes of representative EAFS mixtures are shown in Figure 13.

Figure 11a shows that the EAFS3B mixture exhibited a strength at 28 days of 26.29 MPa, which is relatively low when compared to the strength of the EAFS8B mixture, for the same distribution modulus, q. However, an improvement in the behavior, both in the fresh and in the hardened state, was noted when compared to the EAFS3A mixture. After preparing the EAFS5C mixture, it was found that it would not be advantageous to repeat the EAFS4 mixture for a lower q, since the EAFS4 mixture as the EAFS3A mixture, was very dense and showed poor mechanical properties (Figure 13a,b). The EAFS4 mixture, like the EAFS5C mixture, also contains in its composition a larger number of EAFS aggregate fractions, and the results obtained for the EAFS5C mixture at 28 days show no significant advantages over the EAFS8B and 8C mixtures, which were composed of fewer fractions of EAFS aggregate (less laborious and costly), exhibiting compressive strengths and elasticity modulus as high as the EAFS5C mixture (Figure 11). By comparing the characteristic compressive strength of cylinders at 28 days, it was possible to confirm that the mixtures showing a strength class equal to or higher than the REF1 were the EAFS8B, 8C, 5C and 8D mixtures.

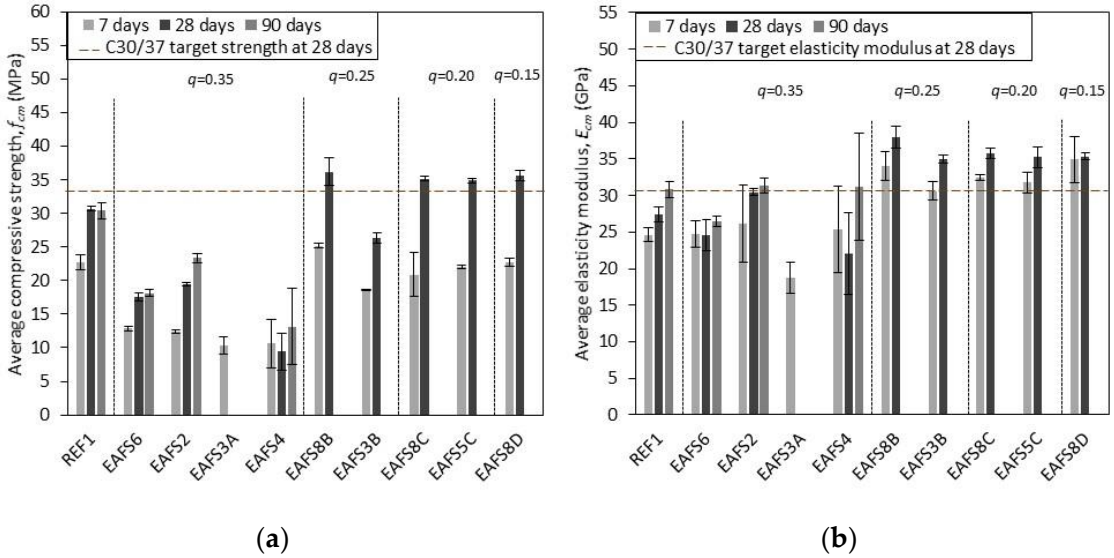
Taking into account the data gathered from the algorithm based on the modified Andreasen and Andersen particle packing model, it was found that the adoption of more EAFS aggregate fractions leads to lower *RSS* values, and the resulting target curves show better agreement. Therefore, it was expected that the EAFS5C mixture at 28 days, as the EAFS mixture with the largest number of EAFS aggregates fractions, would have reached the best compressive strength characteristics. As shown in Figure 11a, the EAFS5C mixture is among the ones showing higher compressive strength, classifiable as C30/37 strength class. However, the EAFS8B, 8C and 8D mixtures at 28 days, with slightly greater values of *RSS*, also showed high values of compressive strength, reaching the strength class obtained with the EAFS5C mixture. It may be concluded that the EAFS8B, 8C and 8D mixtures were more advantageous over the EAFS5C mixture, since good performances in the hardened state were reached with a lower number of EAFS aggregate fractions required, which makes them more practical and economically viable. To some extent, the particularly porous and irregular nature of the EAFS aggregates may justify these results.

The mechanical properties obtained at 90 days were slightly higher than the ones obtained at 28 days after casting (Figure 11), except for EAFS6, which did not contain FA additions. As commonly accepted, one of the characteristics of the FA is to confer

additional strength in the long term, and at 90 days the effect of this type of addition is already observed.

Figure 11a,b show that the EAFS mixtures with a distribution modulus equal to 0.35 did not reach desirable characteristics in terms of strength and stiffness, since according to Eurocode 2 [58] the average values of concrete cylinder compressive strength and elasticity modulus for a strength class C30/37 are 38 MPa and 33 GPa, respectively. On the other hand, EAFS mixtures with a distribution modulus equal to 0.20, 0.25 and 0.15 were much closer or even reached the mechanical requirements, except for EAFS3B.

Considering the fresh behavior of EAFS8B, EAFS8C, and EAFS8D mixtures and by analyzing the results shown in Figure 11a,b at 28 days, it was possible to note that EAFS8C and 8D mixtures were the ones, with high cement amount, that best meet the reference structural concrete properties (REF1). These showed a favorable fresh behavior, with slump class S2/S3, and reached a strength class C30/37. In the design of both EAFS mixtures a cement quantity of 257 kg was used, this amount being smaller than REF1 (280 kg). With this reduction in cement and considering that the EAFS 8C and 8D mixtures contained less fractions of EAFS aggregates, the objectives of producing a structural concrete comparable to a conventional one in terms of deformability and durability, seem feasible and are economically advantageous and environmentally more efficient.



(**a**) (**b**)

Figure 11. Mechanical testing results at 7, 28 and 90 days after casting for REF1 and EAFS mixtures with high cement amount: (**a**) average compressive strength, f_{cm}; (**b**) average elasticity modulus, E_{cm}.

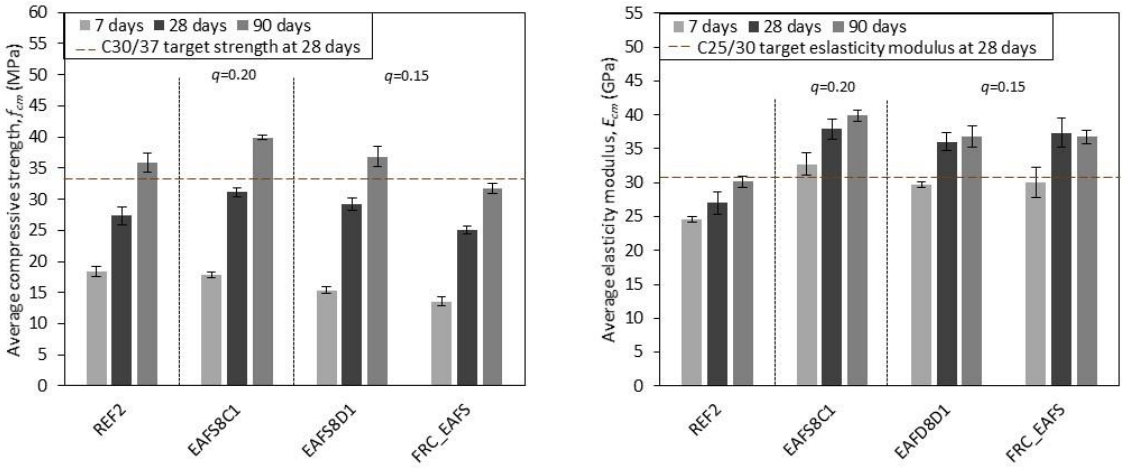
With respect to the percentage of EAFS aggregates of the abovementioned mixtures, 8C and 8D, it is noted that the lower the distribution modulus, the lower the coarse aggregate quantities and consequently the higher the quantity of fine aggregates required. Since the fresh and hardened characteristics of these two mixtures are essentially the same, it was found that the EAFS8C mixture showed to be environmentally more favorable when compared to the EAFS8D mixture, considering the higher percentage of EAFS aggregates present in its composition, which leads to a decrease in the amount of sand required, a natural aggregate that is scarce.

Subsequently, for the mixtures found to be the most advantageous, EAFS8C and 8D, the cement amount was reduced to values similar to that of the REF2 mixture, resulting in the mixtures EAFS8C1 and EAFS8D1. As shown in Figure 12a, both the EAFS8C1 and EAFS8D1 mixtures clearly exceeded the REF2 mixture in terms of strength and deformability, with the compressive strength class of both mixtures equal to C25/30, as shown in Table 10. However, the EAFS8C1 mixture did not reach the S4 slump class required, when comparing to the REF2 mixture (Figure 9b).

Considering these results, EAFS8D1 was the mixture selected to continue with the study of FRC design with RTSF. It reflects the optimal balance between the percentage of EAFS aggregate used and the behavior reached in the fresh and hardened state, therefore showing good potential for the inclusion of the RTSF.

As shown in Table 10 the compressive strength class of EAFS_FRC mixture reduced to C20/25 when compared to EAFS8D1 mixtures (C25/30). In fact, by analyzing Figure 12 it is clear that the fiber reinforced concrete, FRC_EAFS, reached a lower compressive strength than EAFS8D1 and REF2.

This result was somewhat expected, since the RTSF were directly added to the concrete mixture without any previous treatment to separate rubber pieces or other impurities, or separate larger or smaller fibers. Therefore, the fresh behavior of the concrete mixture was significantly impacted by the introduction of the RTSF, as well as the compressive strength and elasticity modulus.



(**a**) (**b**)

Figure 12. Mechanical testing results of REF2, EAFS8C1 and EAFS8D1 mixtures at 7, 28 and 90 days after casting, with lower cement amount: (**a**) average compressive strength, f_{cm}; (**b**) average elasticity modulus, E_{cm}.



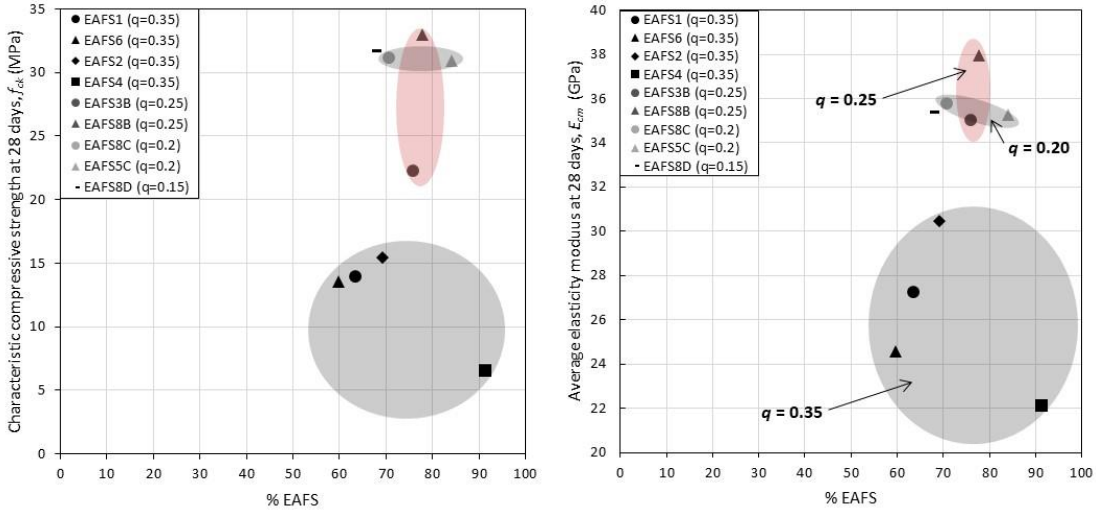
(**a**) (**b**) (**c**) (**d**) (**e**)

Figure 13. Failure modes obtained after compression tests: (**a**) failure mode of EAFS3A mixture; (**b**,**c**) failure mode of EAFS4 mixture; (**d**,**e**) representative failure modes of EAFS6, 2, 8B, 3B, 8C, 5C, 8C1, 8D and 8D1 mixtures in accordance with the satisfactory failure modes of the standard [47].

4.2.2. Optimal Parameters for Designing EAFS Concrete Based on the Andreasen and Andersen Particle Packing Model

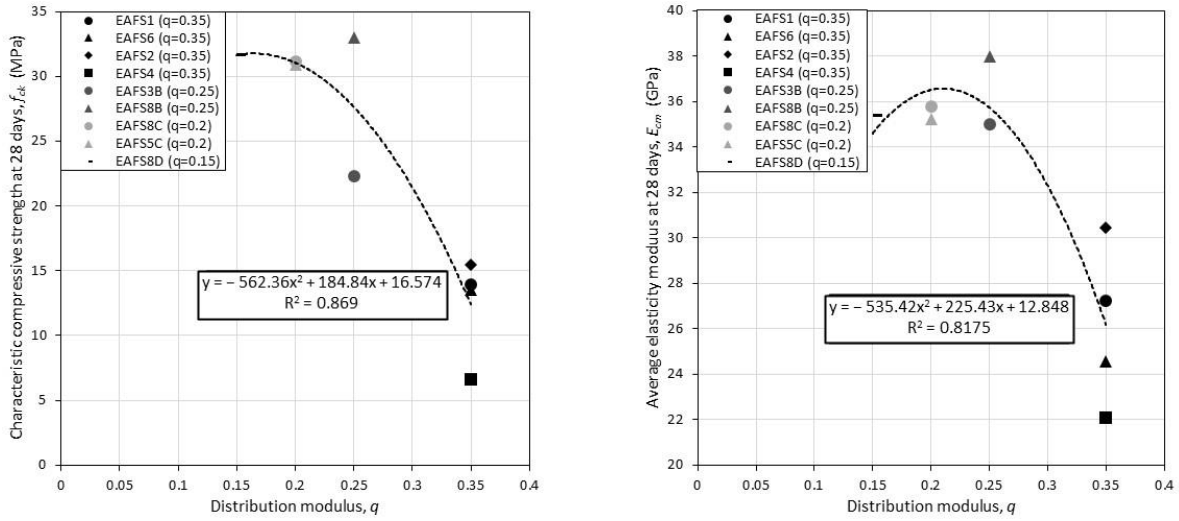
Considering the results obtained when designing EAFS concrete mixtures adopting the modified Andreasen and Andersen particle packing model, it is important to further understand how the different design variables influenced the results obtained. Of particular interest are the percentage of EAFS aggregates added, the water/powder ratio, w/p, and the distribution modulus, q. As shown in Figure 14, for a q value of 0.35, as the percentage of EAFS increases, the characteristic compressive strength and elasticity modulus also increases. The reverse happens for high percentages of EAFS, where the characteristic compressive strength and elasticity modulus starts to decrease. The last may be justified, due to the decrease in paste compared to the amount of EAFS aggregates, which is not enough to obtain such a compact solid skeleton. As the q increases to 0.25, both the characteristic compressive strength and elasticity modulus increases substantially. Note that, despite the two EAFS3B and EAFS8B mixtures being very similar, the mixture EAFS3B has lower characteristic compressive strength and elasticity modulus. As the EAFS3B mixture has a greater variety of EAFS grain size fractions, the resulting paste had a higher amount of EAFS fines (<125 µm) and less CEM and FA compared to the resulting paste of EAFS8B. The EAFS8B mixture has only two EAFS grain size fractions, which means that it has a lower amount of EAFS fines than in the EAFS3B mixture, and therefore, a paste that is richer in CEM and FA, making its solid skeleton stronger. On the other hand, if the value of q decreases by 0.20 or 0.15, the characteristic compressive strength and elasticity modulus will be approximately similar, independent of the EAFS amounts added. This means that an optimal value of q has been reached. This optimal value is lower than what was expected when using conventional aggregates (q = 0.30) perhaps due to the porous nature and angular shape of the EAFS aggregate particles, which appear to require a greater amount of paste [59,60]. For mixtures with a q value equal to 0.20 it is verified what was explained above about the mixtures with higher EAFS grain size factions having lower characteristic compressive strength and elasticity modulus because they have a paste with more EAFS powder fine particles. In this case, this happens for the mixtures EAFS5C (with higher grain size fractions of EAFS) and EAFS8C (with only two grain size fractions of EAFS), however, this difference is not so pronounced for a value of q equal to 0.20. From these findings it can be stated that there is an optimal value of q that depends on the EAFS percentage. This EAFS percentage comes from achieving a balance between the amount of EAFS particle size fineness in the EAFS mixture paste and EAFS aggregates. The higher the value of q, the lower the amount of paste and the higher the amount of aggregates, and therefore, the lower the strength and the elasticity modulus. On the contrary, the smaller the value of q, the greater the amount of paste present in the mixture and the smaller the amount of aggregates, which makes the solid skeleton more compact and stronger. However, if the value of q drops below 0.15, both the strength and the elasticity modulus have a decreasing tendency, that is, for a value of q that is too low there will be a large amount of paste for a small amount of aggregates, and therefore, these small amounts of aggregates are not enough to form a strong solid skeleton.

The evolution of characteristic compressive strength, f_{ck}, and average elasticity modulus at 28 days, E_{cm}, for different q is represented in Figure 15. Based on designed EAFS mixtures it was possible to correlate the different distribution modulus with the characteristic compressive strength and elasticity modulus through a second-degree polynomial equation. As it was already verified for high q values that the strength and elastic modulus tends to decrease, this deduction is possible by using the equation referred to in Figure 15 for EAFS aggregate mixtures. The second-degree polynomial equation also shows that from a certain value of q the strength and elastic modulus will not increase any more but must decrease if q becomes too low.



(a) **(b)**

Figure 14. Mechanical behavior as function of the amount of EAFS aggregates at 28 days: (**a**) characteristic compressive strength, f_{ck}; (**b**) average elasticity modulus, E_{cm}.



(a) **(b)**

Figure 15. Evolution of the mechanical behavior as function of distribution modulus, q, at 28 days: (**a**) characteristic compressive strength, f_{ck}; (**b**) average elasticity modulus, E_{cm}.

The w/p can be correlated to the distribution modulus, q, characteristic compressive strength, f_{ck}, and average elasticity modulus at 28 days, E_{cm}, as shown in Figures 16 and 17, respectively. For this type of aggregate the mixtures show, as expected, that for greater q values the w/p increase according to a linear relation represented in Figure 16. Moreover, for high w/p values, the characteristic compressive strength and elasticity modulus will be smaller, according to the linear relation shown in Figure 17. It should be noted that, the linear regression has a maximum coefficient of determination (R^2) of 62% for the relation of q with w/p ratio (Figure 16), and of 71% and 56% for the relation of the characteristic compressive strength with w/p ratio and elasticity modulus with w/p ratio, respectively. That means that there is a small deviation of the w/p ratio values of the EAFS mixtures from the optimal w/p ratio. However, it can be stated that this difference is due to the different amounts of EAFS particle size fineness that the different EAFS grain size fractions have, that is, it may be necessary to increase or decrease the w/p ratio so that different EAFS

compositions reach the same workability as the reference mixtures, keeping the amount of *SP* equal between them.

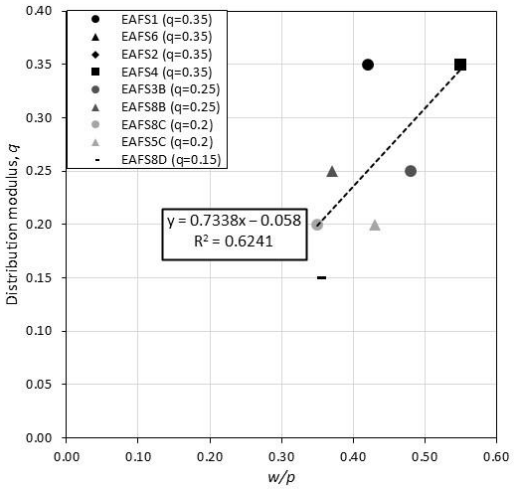
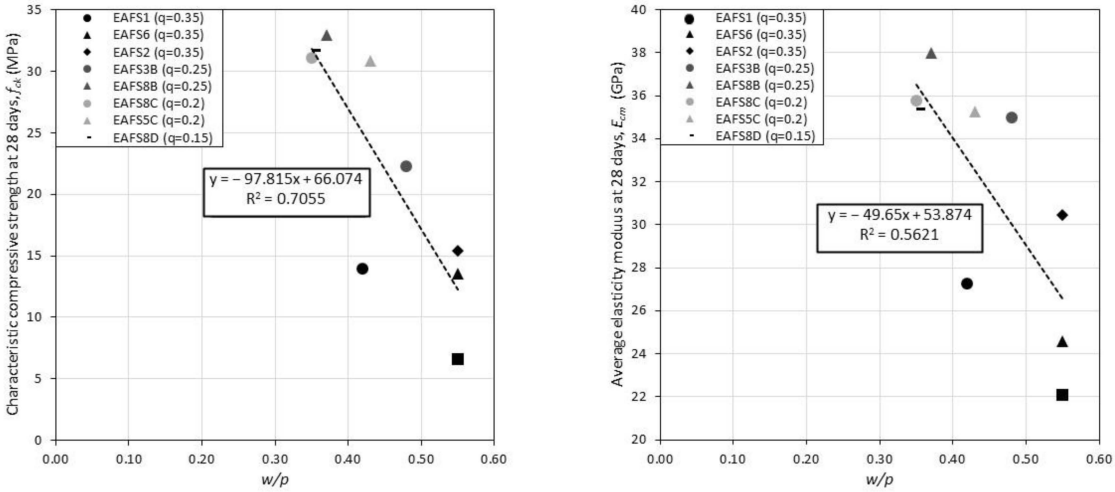


Figure 16. Evolution of distribution modulus, q, with respect to the water/powder ratio, w/p.



(**a**) (**b**)

Figure 17. Evolution of the mechanical behavior with respect to the water/powder ratio, w/p, at 28 days: (**a**) characteristic compressive strength, f_{ck}; (**b**) average elasticity modulus, E_{cm}.

In conclusion it can be said that, according to the modified Andreasen and Andersen particle packing model and within the limits of the current investigation, parameters such as w/p and q may be approximately deduced adopting the linear and second-degree polynomial equations described before. These expressions are valid within the domain $q \in [0.15, 0.35]$ and it may be assumed that similar relationships may be obtained by conducting similar studies for alternative materials. The quantity of EAFS waste aggregates can additionally be reflected as shown in Figure 14.

4.3. Physical Properties

4.3.1. Porosity

Figure 18a shows the results obtained for water absorption by immersion at atmospheric pressure. Mixture FRC_EAFS demonstrated slightly higher open porosity than EAFS8D1 (12.1%) whereas REF2 shows a smaller open porosity compared with EAFS8D1 (25.1%). The average porosity of FRC_EAFS, EAFS8D1 and REF2 were, respectively, 16.2%,

14.5% and 11.6%. Previous studies indicated porosity values for ordinary concretes between 10.4–20.2% [61,62] and for concretes made with fine recycled concrete aggregates between 13.2–16.5%, being 17–46% higher than their reference concrete [63]. This allows us to conclude that the addition of industrial by-products and recycled fibers did not cause a significant increase in the open porosity, in the context of water absorption, and that the slight increase observed with respect to the reference mixture may be associated to the highly porous nature of EAFS aggregates.

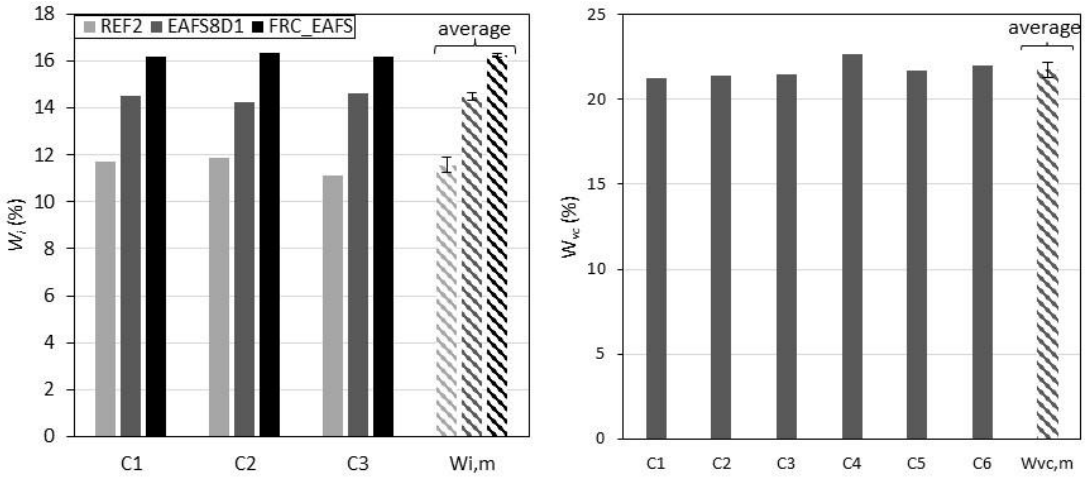


Figure 18. Results of water absorption by immersion: (**a**) for REF2, EAFS8D1 and FRC_EAFS mixtures at atmospheric pressure; (**b**) for EAFS8D1 under vacuum.

Figure 18b presents the test results of water absorption by immersion under vacuum, which indicates that the average open porosity of the EAFS8D1 mixture was 21.8%. Comparing the results obtained in vacuum with the values of open porosity obtained at atmospheric pressure, a higher porosity was obtained as expected. Prior studies showed results of water absorption by immersion under vacuum varying between 11.9–17.9% for ordinary concretes [61,64] and between 9–13% for concretes with bottom ashes or fly ashes as cement replacement [65]. In the present case, the open porosity under vacuum showed slightly higher values, which can again be justified due to the porous nature of EAFS aggregates. The study of alkali-activated ceramic/slag-based mortar showed an open porosity under vacuum of 23.26% [66], which emphasizes that the use of porous materials leads to an open porosity under vacuum higher than other current materials.

4.3.2. Sorptivity

Figure 19 represents the amount of water absorbed by capillarity per unit area versus square root of time. According to Coutinho J. [67] the quality of the concrete can also be measured depending on the capillarity water absorption coefficient (*S*), which corresponds to the slope of the curves represented in Figure 19 during the initial 4 h of testing. The obtained values of *S* were 0.0747 mg/mm^2.min$^{0.5}$ for REF2, 0.1704 mg/mm^2.min$^{0.5}$ for EAFS8D1 and 0.1055 mg/mm^2.min$^{0.5}$ for FRC_EAFS, which according by Browne, R. D. (1991) cited in Camões [62] are typical of high-quality concrete in the case of REF2 and FRC_EAFS, and medium quality concrete in the case of EAFS8D1. The higher capillarity water absorption coefficient of EAFS8D1 can be justified by the porous nature of EAFS aggregates, which represent 70.4% of the total solid ingredient content of the mixture. The material has a high capillarity and reduces open porosity when the diameters of accessible pores are reduced and, conversely, when the diameters are large, the capillarity is reduced, and the open porosity is high. FRC_EAFS showed smaller capillarity compared to

EAFS8D1, perhaps because of the RTSF incorporation and the presence of rubber residue, which may contribute to slightly reduce the permeability.

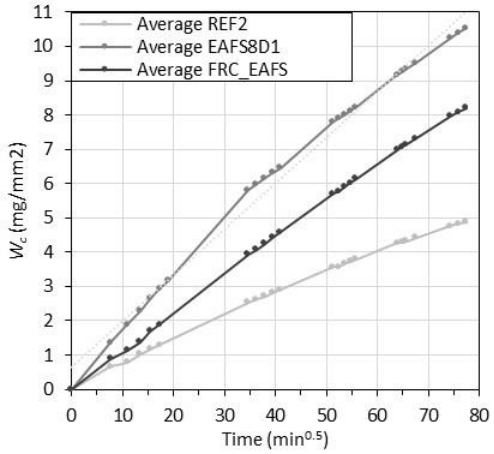


Figure 19. Results of water absorption by capillarity for REF2, EAFS8D1 and FRC_EAFS mixtures.

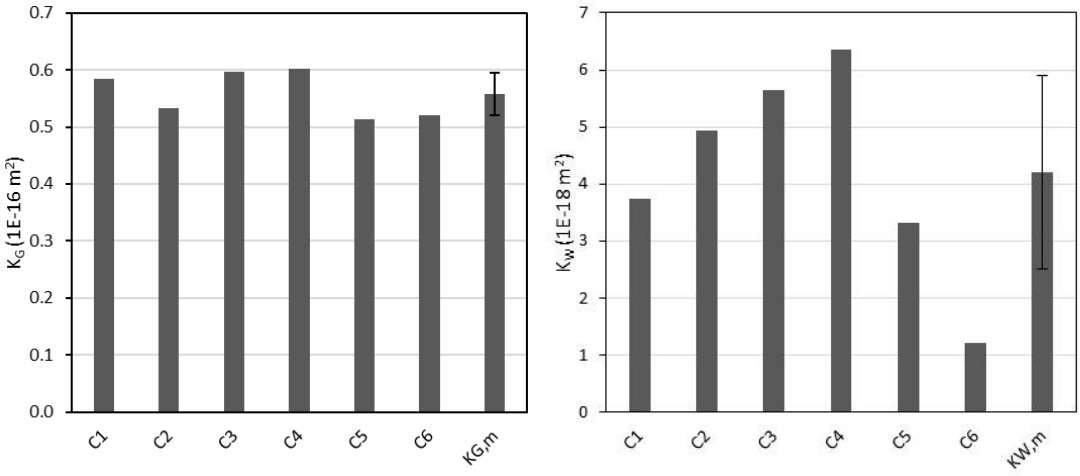
4.3.3. Permeability to Air and Water

As shown in Tables 16 and 17, the coefficients of variation of air and water permeability were 6.7% and 40.1%, respectively. Some authors suggest that for concretes with w/c ratio below 0.53, the coefficient of variation (CoV) is small, and six samples are sufficient, while for concretes with a w/c ratio above 0.65, the CoV is large, and it is necessary to increase the number of samples to consider the increase in concrete heterogeneity translated by a higher CoV. They also noted that a CoV of up to 20% is considered acceptable for air and water permeability coefficients, K_G and K_W [61,68]. In this study, the CoV of air permeability coefficient was within the order of magnitude of the CoV expected for that type of test, while in the case of water permeability coefficient the CoV result was higher. Probably the higher CoV obtained for water permeability coefficient can be justified by the use of EAFS aggregates, which made the concrete matrix more heterogeneous due to its irregularity and porosity, and therefore it is recommended to increase the number of test samples to reduce the CoV.

Figure 20 shows the air and water permeability coefficients obtained. The average air and water permeability coefficients were, respectively, 0.558×10^{-16} and 4.20×10^{-18} m^2. For conventional concretes and concretes with higher amounts of bottom or fly ash, of a strength class C25/C30, other studies found K_G values between 0.39–0.88 $\times 10^{-16}$ m^2, which was in accordance with the K_G value obtained in the present study [64,65,69]. By comparing the K_W value obtained with other studies, it was found that for conventional and higher amount of FA concretes of a strength class C25/C30 values of 6.4 and 2.16×10^{-18} m^2 were obtained [61,64]. Hence, the result of K_W determined in this research was in accordance with the literature. It is possible to classify qualitatively the concrete based on the coefficient of water permeability, using the classification proposed by Coutinho J. [67] according to the Table 21. In this way, the EAFS8D1 mixture can be classified as a concrete of normal quality in terms of water permeability.

Table 21. Quality class of concrete as a function of its water permeability coefficient.

Water Permeability Coefficient, K_W (m/s)	Water Permeability Coefficient, K_W (m^2)	Quality Class
$\geq 1 \times 10^{-10}$	$\geq 1.3 \times 10^{-17}$	Reduced
1×10^{-12}–1×10^{-10}	1.3×10^{-19}–1.3×10^{-17}	Normal
$\leq 1 \times 10^{-12}$	$\leq 1.3 \times 10^{-19}$	High



(a) **(b)**

Figure 20. (**a**) results obtained for air permeability coefficient, K_G, for EAFS8D1 mixture; (**b**) results obtained for water permeability coefficient, K_W, for EAFS8D1 mixture.

4.3.4. Resistance to Carbonation

Figure 21 shows the average results of the accelerated carbonation test of concrete samples REF2, EAFS8D1 and FRC_EAFS for up to 186 days of exposure. The depth of carbonation can be expressed as a function of the square root of the exposure time, typically resulting in a linear trend of evolution. The slope of the linear trend corresponds to the carbonation coefficient, K_c, which, as shown in Figure 21, were 2.86, 2.61 and 2.41 mm/day$^{0.5}$ for the REF2, EAFS8D1 and FRC_EAFS mixtures, respectively. This means that the carbonation coefficient of the REF2 mixture was 9.4% higher when compared to the carbonation coefficient of the EAFS8D1 mixture, and the carbonation coefficient of the EAFS8D1 mixtures was 8.6% higher when compared to the carbonation coefficient of FRC_EAFS. This indicates that the REF2 mixture was more susceptible to carbonation than the EAFS8D1 mixture, and the EAFS8D1 mixture was more susceptible to carbonation than FRC_EAFS.

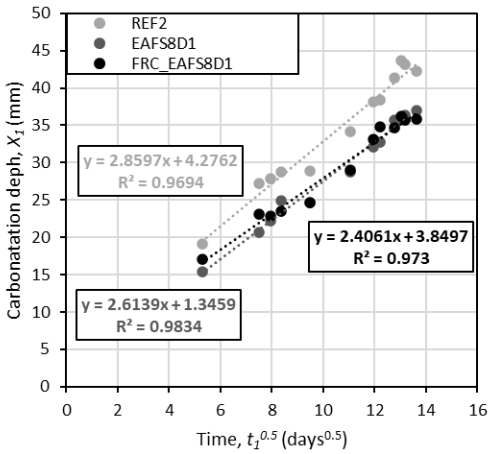


Figure 21. Results of carbonation depth along exposed time for REF2, EAFS8D1 and FRC_EAFS mixtures.

As shown in Table 20, the variation of the average carbonation resistance, R_{c65m}, from REF2 to EAFS8D1 was 25.1% smaller, which corroborates the observations made at the surface of REF2 mixture specimens that showed a greater progress depth of the carbonation front (Table 18). The same conclusion can be drawn for the EAFS8D1 mixture, which has an

average carbonation resistance, R_{c65m}, 3% smaller than FRC_EAFS mixture; however, this difference is almost insignificant. Thus, somewhat contrasting to what was expected based on the previous results of water absorption at atmospheric pressure and by capillarity, the EAFS8D1 and FRC_EAFS mixtures show higher carbonation resistance than the reference mixture REF2 does in the uncracked state. This can be explained due to the changing of calcium hydroxide ($Ca(OH)_2$) into calcium carbonate ($CaCO_3$) by the uptake of CO_2. The expansion of the solid volume inside the concrete caused by the portlandite ($Ca(OH)_2$) carbonatation partially filled the free pores [70–72]. Since in the case of the EAFS8D1 and FRC_EAFS mixtures the porosity and sorptivity were greater than REF2, the reaction products resulting from the accelerated carbonatation test in the EAFS8D1 and FRC_EAFS mixtures were also greater. In this way, the EAFS8D1 and FRC_EAFS mixtures could exhibit an improved behavior to potential carbonation resistance relative to the REF2 mixture. That process can be confirmed by performing water absorption and sorptivity tests after submitting both mixtures to accelerated carbonation test, where porosity and sorptivity should be lower than the results obtained previously in the uncarbonated state. This porosity and sorptivity reduction should be more significant in the case of the EAFS8D1 and FRC_EAFS mixtures. Another reason for the EAFS mixtures presenting an enhanced carbonatation resistance behavior in relation to the reference mixture REF2 is the released of Ca^+ ions from the EAFS' Ca-bearing phases, which reacted with CO_2 forced into the microstructure. This reaction resulted in the precipitation of $CaCO_3$, which significantly densified the microstructure, and as explained above, partially filled the free pores [73].

5. Conclusions

The present research was aimed at studying the design approach for structural concrete mixtures with the incorporation of wastes. In particular, electric arc furnace slag (EAFS) aggregates and fly ash (FA) powder, as well as recycled tire waste (RTSF) were used and the developed matrixes were compared with two reference mixtures, REF1 and REF2. According to the predefined requirements of the two target mixtures and by using the modified Andreasen and Andersen particle packing model, it was possible to achieve EAFS optimized concrete compositions, reaching the highest compactness and strength. RTSF were also incorporated in the EAFS concrete selected in order to assess the feasibility of developing FRCs including high wastes percentages. Workability and mechanical behavior were evaluated for reference mixtures, REF1 and REF2, and for the designed EAFS mixtures developed with and without RTSF. Physical properties were investigated for EAFS8D1, FRC_EAFS and the reference mixture REF2, as representatives of the studied mixtures. The FRC_EAFS allowed to study the effect of the incorporation of RTSF on the physical properties of the designed mixtures. The main conclusions of this study are:

(1) The EAFS aggregates significantly altered the concrete fresh state when compared to natural aggregates typically used in structural concrete design. Compositions have been shown to be very sensitive to the process of mixing and to the w/p or w/c ratio, most likely due to the porous nature of the EAFS aggregates. The EAFS aggregates' porosity leads to the delayed absorption of water during the mixing process, resulting in alterations of the fresh and hardened behavior during mixing that could be solved by adapting the mixing process.

(2) Two of the mixtures of greater interest for a waste-based structural concrete were the EAFS8C and EAFS8D1 mixtures, which reflected the optimal balance between the percentage of EAFS aggregate used and the behavior reached in the fresh and hardened state. Nevertheless, the EAFS8D1 mixture seemed to be a more sustainable mixture, since the amount of cement used in its composition was approximately 19% lower than the EAFS8C mixture. The replacement of a significant portion of the natural ingredients with substantial quantities of industrial by-products increases the sustainability potential of concrete, in particular with the EAFS8D1 mixture. The replacement percentages (in weight of solid ingredients) were about 10% of FA and 70% of EAFS aggregates.

(3) For a structural concrete containing EAFS aggregates, the results seemed to indicate that parameters w/p and q can be initially estimated for intermediate values of the parameters studied adopting the linear and second-degree polynomial equations.

(4) The average air and water permeability coefficients of EAFS8D1 were in accordance with the values found in the literature. Moreover, based on water permeability coefficients, K_W, the EAFS8D1 mixture can be classified as a concrete of normal quality by using the classification proposed by Coutinho J. [59].

(5) The carbonation coefficient of REF2 mixture was 9.4% higher compared with the carbonation coefficient of the EAFS8D1 mixture, and the variation of the average carbonation resistance, R_{c65m}, of REF2 was 25.1% lower than EAFS8D1. FRC_EAFS showed even better results, when compared to REF2. In this way, the EAFS8D1 and FRC_EAFS mixtures showed an improved behavior to carbonation resistance relative to the reference mixture.

By adopting the design approach followed, it was possible to design concrete mixtures that, while meeting the fresh and hardened state requirements, were able to incorporate large percentages of wastes or industrial by-products, and therefore potentially improve environmental performance. The mixtures developed even outperformed the conventional reference mixtures in some of their characteristics, such as strength and resistance to carbonation. Therefore, the methodology studied showed great potential to be used as a standard approach to maximize wastes and industrial by-products incorporation in structural concrete. In particular, EAFS showed interesting characteristics to be used as aggregate, impacting positively both the mechanical properties and the carbonation resistance.

Author Contributions: Conceptualization, A.N., T.M., V.M.C.F.C., M.R., J.C. and E.B.P.; Methodology, A.N, J.A., F.C., T.M., V.M.C.F.C. and E.B.P.; Formal analysis, A.N. and E.B.P.; Investigation, A.N.; Resources, M.R., J.C., E.B.P.; Writing–original draft, A.N.; Writing–review & editing, A.N., T.M., V.M.C.F.C. and E.B.P.; Supervision, T.M. and E.B.P.; Project administration, T.M., V.M.C.F.C., M.R., J.C. and E.B.P.; Funding acquisition, T.M., V.M.C.F.C. and E.B.P. All authors have read and agreed to the published version of the manuscript.

Funding: This research was funded by Fundação para a Ciência e a Tecnologia grant number SFRH/BD/135790/2018) and projects with references POCI-01-0247-FEDER-033834, NORTE-01-0145-FEDER-000032.

Institutional Review Board Statement: Not applicable.

Informed Consent Statement: Not applicable.

Data Availability Statement: The data presented in this study are available on request from the corresponding author. The data are not publicly available due to privacy restrictions.

Acknowledgments: The first author would also like to thank FCT (Fundação para a Ciência e a Tecnologia) for the funding through the PhD grant SFRH/BD/135790/2018. The authors would like to thank DST company, the project RENEw, POCI-01-0247-FEDER-033834, funded by Fundo Europeu de Desenvolvimento Regional (FEDER) and Programa Operacional da Competitividade e Internacionalização do Portugal 2020 (COMPETE 2020), "Next generation monitoring of coastal ecosystems in a scenario of global change", NORTE-01-0145-FEDER-000032, funded by Fundo Europeu de Desenvolvimento Regional (FEDER) and Programa Operacional Regional do Norte (NORTE2020), and "CirMat: CIRcular aggregates for sustainable road and building MATerials" is funded by Iceland, Liechtenstein and Norway through the EEA Grants and Norway Grants, operationalized by the Portuguese Office of the Secretary of State for the Environment. They are also very grateful to the companies SECIL and SIKA for the material provided that contributed to the realization of this study.

Conflicts of Interest: The authors declare no conflict of interest.

References

1. Eštoková, A.; Fabiánová, M.W.; Ondová, M. Concrete Structures and Their Impacts on Climate Change and Water and Raw Material Resource Depletion. *Int. J. Civ. Eng.* **2022**, *20*, 735–747. [CrossRef]
2. Dimoudi, A.; Tompa, C. Energy and environmental indicators related to construction of office buildings. *Resour. Conserv. Recycl.* **2008**, *53*, 86–95. [CrossRef]

3. European Commission. *Leading the Way to a Global Circular Economy: State of Play and Outlook Environment*; Publications Office of the European Union: Luxembourg, 2020. [CrossRef]
4. Vu, H.M.; Forth, J.P.; Toropov, V. *The Use of Glycerol and Cooking Oil in Masonry Unit Production*; ICE (Institution of Civil Engineers) Publishing: London, UK, 2015; p. 14. [CrossRef]
5. Yu, R.; Spiesz, P.; Brouwers, H.J.H. Development of an eco-friendly Ultra-High Performance Concrete (UHPC) with efficient cement and mineral admixtures uses. *Cem. Concr. Compos.* **2015**, *55*, 383–394. [CrossRef]
6. Rodrigues, I.P. Ligantes de Baixo Impacto Ambiental e Baixo Custo, Baseados na Ativação Química de Escórias de Aciaria. Master's Thesis, Escola de Engenharia da Universidade do Minho, Guimarães, Portugal, 2015.
7. Ramos, T.; Juvandes, L.; Moreira, A. Utilização de ASIC em betão. In Proceedings of the Encontro Nacional Betão Estrutural-BE2012, Porto, Portugal, 24–26 October 2012; pp. 24–26.
8. Pacheco, A. Estudo da Viabilidade da Utilização de Escórias de Aciaria (ASIC) em Betão Denso. Master's Thesis, Faculdade de Engenharia da Universidade do Porto, Porto, Portugal, 2012.
9. Torgal, F.P.; Jalali, S. Sustentabiliade-Tendências para a sustentabilidade dos materiais de construção. *Eng. Vida* **2008**, *42*, 2–5.
10. Torgal, F.P.; Jalali, S. Eco-Eficiência dos Materiais de Construção. *Rev. Assoc. Port. Empresas Betão Pronto* **2010**, *147*, 48–55.
11. Aiello, M.A.; Leuzzi, F. Waste tyre rubberized concrete: Properties at fresh and hardened state. *Waste Manag.* **2010**, *30*, 1696–1704. [CrossRef] [PubMed]
12. Thomas, B.S.; Gupta, R.C. Long term behaviour of cement concrete containing discarded tire rubber. *J. Clean Prod.* **2015**, *102*, 78–87. [CrossRef]
13. Su, H.; Yang, J.; Ling, T.; Ghataora, G.S.; Dirar, S. Properties of concrete prepared with waste tyre rubber particles of uniform and varying sizes. *J. Clean Prod.* **2015**, *91*, 288–296. [CrossRef]
14. Li, G.; Garrick, G.; Eggers, J.; Abadie, C.; Stubblefield, M.A.; Pang, S. Waste tire fiber modified concrete. *Compos. B Eng.* **2004**, *35*, 305–312. [CrossRef]
15. Azevedo, F.; Jesus, C.; de Aguiar, J.L.B.; Camões, A.F. Properties and durability of HPC with tyre rubber wastes. *Constr. Build. Mater.* **2012**, *34*, 186–191. [CrossRef]
16. Bari, A.; Jel, M.; Pezer, M.; Nina, Š. Influence of recycled tire polymer fibers on concrete properties. *Cem. Concr. Compos.* **2018**, *91*, 29–41. [CrossRef]
17. Sousa Coutinho, A. *Fabrico e Propriedades do Betão*; LNEC-Laboratorio Nacional de Engenharia Civil: Lisbon, Portugal, 1988; Volume 1.
18. CPPE-Companhia Portuguesa de Produção de Electricidade SA (Grupo EDP). Cinzas Volantes-Aplicações em Cimentos e Betões. *Boletim da Sociedade Portuguesa de Química, Correntes de Despolorização Termostimuladas*, March 1995. Available online: https://www.spq.pt/magazines/BSPQuimica/580/article/3000681/pdf (accessed on 1 November 2022).
19. Torgal, F.P.; Jalali, S. *Betão Eco-Eficiência: O Futuro da Indústria do Betão Pronto*; Associação Portuguesa das Empresas de Betão Pronto: Amadora, Portugal, 2011; Volume 26, pp. 22–27.
20. Andrade, R.M.A. Caracterização Laboratorial de Misturas Betuminosas com Incorporação de Agregado Siderúrgico Inerte para Construção (ASIC). Master's Thesis, Instituto Superior de Engenharia de Lisboa, Lisbon, Portugal, 2015.
21. Arribas, I.; Santamaría, A.; Ruiz, E.; Ortega-López, V.; Manso, J.M. Electric arc furnace slag and its use in hydraulic concrete. *Constr. Build. Mater.* **2015**, *90*, 68–79. [CrossRef]
22. Santamaría, A.; Ortega-López, V.; Skaf, M.; Marcos, I.; San-José, J.T.; González, J.J. Performance of hydraulic mixes manufactured with electric arc furnace slag aggregates. In Proceedings of the 3rd Pan American Materials Congress, San Diego, CA, USA, 26 February–2 March 2017; No. 9783319521312. pp. 227–234. [CrossRef]
23. San-José, J.T.; Vegas, I.; Arribas, I.; Marcos, I. The performance of steel-making slag concretes in the hardened state. *Mater. Des.* **2014**, *60*, 612–619. [CrossRef]
24. Papayianni, I.; Anastasiou, E. Utilization of electric arc furnace steel slags in concrete products. In Proceedings of the 6th European Slag Conference, Madrid, Spain, 20–22 October 2010; pp. 319–334. Available online: https://www.researchgate.net/publication/255965247 (accessed on 4 January 2023).
25. Arribas, I.; Vegas, I.; San-José, J.T.; Manso, J.M. Durability studies on steelmaking slag concretes. *Mater. Des.* **2014**, *63*, 168–176. [CrossRef]
26. Manso, J.M.; Gonzalez, J.J.; Polanco, J.A. Electric Arc Furnace Slag in Concrete. *J. Mater. Civ. Eng.* **2004**, *16*, 639–645. [CrossRef]
27. García-Cortés, V.; Estévez, D.G.; San-José, J.T. Assessment of particle packing models for aggregate dosage design in limestone and EAFS aggregate-based concretes. *Constr. Build. Mater.* **2022**, *328*, 126977. [CrossRef]
28. Chatzopoulos, A.; Sideris, K.K.; Tassos, C. Production of concretes using slag aggregates: Contribution of increasing the durability and sustainability of constructions. *Case Stud. Constr. Mater.* **2021**, *15*, e00711. [CrossRef]
29. González-Ortega, M.A.; Cavalaro, S.H.P.; de Sensale, G.R.; Aguado, A. Durability of concrete with electric arc furnace slag aggregate. *Constr. Build. Mater.* **2019**, *217*, 543–556. [CrossRef]
30. Correia, A.G.; Roque, A.J.; Ferreira, S.F.; Castro, F.; Fortunato, E.; de Santayana, F.P.; Trigo, L. A Valorização de Agregados Siderúrgicos Inertes Reciclados em Obras Geotécnicas-Um Projeto Nacional. *Valorização Resíduos*, Guimarães, Portugal, pp. 19–25, November 2007. Available online: http://repositorio.lnec.pt:8080/jspui/handle/123456789/1004012 (accessed on 4 January 2023).
31. Fazli, A.; Rodrigue, D. Recycling waste tires into Ground Tire Rubber (GTR)/rubber compounds: A review. *J. Compos. Sci.* **2020**, *4*, 103. [CrossRef]

32. Andreasen, A.H.M.; Andersen, J. Über die Beziehung zwischen Kornabstufung und Zwischenraum in Produkten aus losen Körnern (mit einigen Experimenten). *Kolloid-Zeitschrift* **1930**, *50*, 217–228. [CrossRef]
33. Funk, J.E.; Dinger, D. *Predictive Process Control of Crowded Particulate Suspensions: Applied to Ceramic Manufacturing*; Springer: New York, NY, USA, 1994. [CrossRef]
34. Husken, G. A Multifunctional Design Approach for Sustainable Concrete-with Application to Concrete Mass Products. Ph.D. Thesis, Eindhoven University of Technology, Eindhoven, The Netherlands, 2010.
35. Yu, R.; Spiesz, P.; Brouwers, H.J.H. Mix design and properties assessment of Ultra-High Performance Fibre Reinforced Concrete (UHPFRC). *Cem. Concr. Res.* **2014**, *56*, 29–39. [CrossRef]
36. Yu, R.; Tang, P.; Spiesz, P.; Brouwers, H.J.H. A study of multiple effects of nano-silica and hybrid fibres on the properties of Ultra-High Performance Fibre Reinforced Concrete (UHPFRC) incorporating waste bottom ash (WBA). *Constr. Build. Mater.* **2014**, *60*, 98–110. [CrossRef]
37. Yu, R.; Spiesz, P.; Brouwers, H.J.H. Development of Ultra-High Performance Fibre Reinforced Concrete (UHPFRC): Towards an efficient utilization of binders and fibres. *Constr. Build. Mater.* **2015**, *79*, 273–282. [CrossRef]
38. Yu, R.; Spiesz, P.; Brouwers, H.J.H. Effect of nano-silica on the hydration and microstructure development of Ultra-High Performance Concrete (UHPC) with a low binder amount. *Constr. Build. Mater.* **2014**, *65*, 140–150. [CrossRef]
39. Yu, R.; Spiesz, P.; Brouwers, H.J.H. Static properties and impact resistance of a green Ultra-High Performance Hybrid Fibre Reinforced Concrete (UHPHFRC): Experiments and modeling. *Constr. Build. Mater.* **2014**, *68*, 158–171. [CrossRef]
40. Yu, Q.L.; Spiesz, P.; Brouwers, H.J.H. Cement & Concrete Composites Ultra-lightweight concrete: Conceptual design and performance evaluation. *Cem. Concr. Compos.* **2015**, *61*, 18–28. [CrossRef]
41. Yu, R.; Van Onna, D.V.; Spiesz, P.; Yu, Q.L.; Brouwers, H.J.H. Development of Ultra-Lightweight Fibre Reinforced Concrete applying expanded waste glass. *J. Clean Prod.* **2016**, *112*, 690–701. [CrossRef]
42. *ASTM C 566-97*; Standard Test Method for Total Evaporable Moisture Content of Aggregate by Drying. ASTM International Standarts: West Conshohocken, PA, USA, 2004; p. 3.
43. *EN 12390-1*; Testing Hardened Concrete-Part 1: Shape, Dimensions and Other Requirements for Specimens and Moulds. European Standard: Brussels, Belgium, 2012; pp. 1–14.
44. *EN 12390-2*; Testing Hardened Concrete-Part 2: Making and Curing Specimens for Strength Tests. European Standard: Brussels, Belgium, 2009; p. 8.
45. *EN 12350-2*; Testing Fresh Concrete-Part 2: Slump-Test. European Standard: Brussels, Belgium, 2009; p. 8.
46. *EN 12390-13*; Testing Hardened Concrete-Part 13: Determination of Secant Modulus of Elasticity in Compression. European Standard: Brussels, Belgium, 2013; p. 14. [CrossRef]
47. *EN 12390-3*; Testing Hardened Concrete-Part 3: Compressive Strength of Test Specimens. European Standard: Brussels, Belgium, 2009; p. 21.
48. *LNEC E 394*; Determination of the Absorption of Water by Immersion. Laboratório Nacional de Engenharia Civil: Lisbon, Portugal, 1993.
49. *LNEC E 395*; Determination of the Absorption of Water by Immersion under Vacuum. Laboratório Nacional de Engenharia Civil: Lisbon, Portugal, 1993.
50. *LNEC E 393*; Determination of the Absorption of Water through Capillarity. Laboratório Nacional de Engenharia Civil: Lisbon, Portugal, 1993.
51. Rilem, T.C. CPC 11.1 Absorption of water by immersion. In *RILEM Recommendations for the Testing and Use of Constructions Materials*; Rilem, E., Sponed, F.N., Eds.; Springer: Berlin, Germany, 1994; p. 33. [CrossRef]
52. Rilem, T.C. CPC 11.2 Absorption of water by capilarity. In *RILEM Recommendations for the Testing and Use of Constructions Materials*; Rilem, E., Sponed, F.N., Eds.; Springer: Berlin, Germany, 1994; pp. 34–35. [CrossRef]
53. Rilem, T.C. CPC 11.3 Absorption of water by concrete by immersion under vacuum. In *RILEM Recommendations for the Testing and Use of Constructions Materials*; Rilem, E., Sponed, F.N., Eds.; Springer: Berlin, Germany, 1994; Volume 17, pp. 36–37. [CrossRef]
54. Cabrera, J.G. Design an Productionb of High Performance Durable Concrete. In Proceedings of the International Conference: Infrastructure Regeneration and Rehabilitation Inproving the Quality of Life through Better Cronstruction-A Vision for the Next Millennium, Sheffield, UK, 28 June–2 July 1999; Sheffield Academic Press: Sheffield, UK, 1999; pp. 1–14.
55. *BS 1881-210*; Testing Hardened Concrete-Part 210: Determination of the Potential Carbonation Resistance of Concrete-ACCELERATED Carbonation Method. European Standard: London, UK, 2013; p. 14.
56. *NP EN 206-1*; Concrete-Part 1: Specification, Performance, Production and Conformity. European Standard: Brussels, Belgium, 2000; p. 84.
57. *LNEC E 465*; Betões. Metodologia para Estimar as Propriedades de Desempenho do Betão que Permitem Satisfazer a Vida útil de Projecto de Estruturas de Betão Armado ou Pré-Esforçado Sob as Exposições Ambientais XC e XS. Laboratório Nacional de Engenharia Civil: Lisbon, Portugal, 2007; pp. 1–24.
58. *EN 1992-1-1*; Design of Concrete Structures-Part 1-1: General Rules and Rules for Buildings. European Standard: Brussels, Belgium, 2004; p. 230.
59. Freitas, N.E.D. *Sustentabilidade de Estruturas de Betão em Ambiente Marítimo com Recurso a FRP*; Escola de Engenharia da Universidade do Minho: Guimarães, Portugal, 2016.

60. Pereira, J. *Dissertação de Mestrado em Engenharia Civil-Estruturas de Betão Reforçadas com Materiais Compósitos em Ambiente Marítimo e Concebidas com Água do Mar*; Escola de Engenharia da Universidade do Minho: Guimarães, Portugal, 2016.
61. Ferreira, R.M. Avaliação de Ensaios de Durabilidade do Betão. Master's Thesis, Universidade do Minho, Guimarães, Portugal, 2000.
62. Camões, A. Betões de Elevado Desempenho com Incorporação de Cinzas Volantes. Ph.D. Thesis, University of Minho, Guimarães (Portugal), Guimarães, Portugal, 2002.
63. Evangelista, L.; de Brito, J. Durability performance of concrete made with fine recycled concrete aggregates. *Cem. Concr. Compos.* **2010**, *32*, 9–14. [CrossRef]
64. Camões, A. *Betões de Elevado Desempenho com Elevado Volume de Cinzas Volantes*; Universidade do Minho: Guimarães, Portugal, 2005.
65. Martins, I.M.; Gonçalves, A.; Marques, J. Durability and Strength Properties of Concrete Containing Coal Bottom Ash. In Proceedings of the pro077: International RILEM Conference on Material Science, Aachen, Germany, 6–10 September 2010; pp. 275–283. Available online: http://eprints.whiterose.ac.uk/76421/ (accessed on 10 February 2021).
66. Gaibor, N.; Leitão, D.; Miranda, T.; Cristelo, N.; Pereira, E.N.B.; Cunha, V.M.C.F. Effect of polyacrylonitrile fiber on the properties of alkali-activated ceramic/slag-based mortar. *J. Build. Eng.* **2021**, *44*, 103367. [CrossRef]
67. Coutinho, J.D.S. Melhoria da Durabilidade dos Betões Por Tratamento da Cofragem. Ph.D. Thesis, Universidade do Porto, Porto, Portugal, 1998.
68. Hassan, K.E.; Cabrera, J.G. Control of concrete performance by limiting oxygen permeability and oxygen diffusion. In Proceedings of the International Conference: Infrastructure Regeneration and Rehabilitation Inproving the Quality of Life through Better Cronstruction—A Vision for the Next Millennium, Sheffield, UK, 28 June–2 July 1999; Sheffield Academic Press: Sheffield, UK, 1999; pp. 1085–1095.
69. Ferreira, R.M.; Jalali, S. *Avaliação dos Ensaios Correntes para a Medição da Durabilidade do Betão*; Universidade do Minho: Guimarães, Portugal, 2001.
70. De Ceukelaire, L.; van Nieuwenburg, D. Accelerated Carbonation of a Blast-furnace Cement Concrete. *Cem. Concr. Res.* **1993**, *23*, 442–452. [CrossRef]
71. Dias, W.P.S. Reduction of concrete sorptivity with age through carbonation. *Cem. Concr. Res.* **2000**, *30*, 1255–1261. [CrossRef]
72. Gonen, T.; Yazicioglu, S. The influence of compaction pores on sorptivity and carbonation of concrete. *Constr. Build. Mater.* **2007**, *21*, 1040–1045. [CrossRef]
73. Kassim, D.; Lamaa, G.; Silva, R.V.; de Brito, J. Performance Enhancement of Alkali-Activated Electric Arc Furnace Slag Mortars through an Accelerated CO_2 Curing Process. *Appl. Sci.* **2022**, *12*, 1662. [CrossRef]

Disclaimer/Publisher's Note: The statements, opinions and data contained in all publications are solely those of the individual author(s) and contributor(s) and not of MDPI and/or the editor(s). MDPI and/or the editor(s) disclaim responsibility for any injury to people or property resulting from any ideas, methods, instructions or products referred to in the content.